The effect of spiral cold-bending manufacturing process on pipeline mechanical behavior

THE EFFECT OF SPIRAL COLD-BENDING MANUFACTURING PROCESS ON PIPELINE MECHANICAL BEHAVIOR

G. Chatzopoulou [a], G. C. Sarvanis [a], S. A. Karamanos [a, b, 1], E. Mecozzi [c], and O. Hilgert [d]

[a] *Department of Mechanical Engineering, University of Thessaly, Volos, Greece*

[b] *School of Engineering, Institute for Infrastructure & Environment, The University of Edinburgh, Scotland, UK*

[c] *Rina Consulting – Centro Sviluppo Materiali S.p.A., Rome Italy*

[d] *Salzgitter Mannesmann Forschung GmbH, Duisburg, Germany*

ABSTRACT

Large-diameter steel pipes, fabricated through the spiral-welding manufacturing process, are extensively used in onshore pipelines for the transmission of energy (hydrocarbon) and water resources. However, their use in demanding applications, such as geohazard areas or in offshore applications has been very limited. Safeguarding the structural integrity in such areas of those pipes requires an efficient strain-based design framework. Bending deformation capacity in the presence of internal pressure is the major loading case under geohazard actions, whereas external pressure capacity governs the mechanical design in moderate-deep offshore applications. To predict accurately the structural performance of spiral-welded pipes, the cold-bending manufacturing process should be taken into account. In the present paper, numerical models are developed simulating both the cold-bending process (decoiling and spiral bending) and the structural response of the pipe subjected to the loading conditions under consideration. The numerical modes have been verified against experimental results of spiral pipes conducted in the framework of a European research project. A parametric analysis is also conducted to examine the effect of spiral cold forming process on the structural behavior of spiral welded pipes. The results from the present study indicate that spiral-welded pipes can sustain significant amount of bending deformation and external pressure, in favor of their use in demanding onshore and moderately deep offshore pipeline applications.

[1] Corresponding author. Email: skara@mie.uth.gr

1 INTRODUCTION

Spiral-welded pipes are popular in large-diameter pipeline applications for hydrocarbon and water transmission due to lower manufacturing cost in comparison with longitudinal welded pipes, e.g. UOE pipes [1]. Spiral welded line pipes are larger than 24 inches in diameter, and are characterized by a relatively large value of diameter-to-thickness ratio D/t ($D/t \geq 40$). However, there is a reluctance of using spiral welded pipes in demanding applications, such as geohazard areas, where the pipeline is subjected to severe ground-inducted actions. Recently, there exists a debate on whether those pipes can also be considered for moderately deep offshore pipeline applications, (up to 500 meters of water depth) as an alternative to longitudinal-seam pipes.

During the last years, research has been carried out in order to investigate the mechanical behavior of spiral welded tubes or pipes under combined bending and internal pressure, employing mainly experimental testing but also numerical approaches. Zimmerman *et al.* [2] presented the results of an extensive experimental and analytical research program to determine the compressive buckling resistance of large-diameter, spiral-welded linepipes and they concluded that spiral welded linepipe is as good as longitudinally welded linepipe in terms of buckling capacity. Van Es *et al.* [3], [4] presented a series of full-scale four-point bending tests on 42-inch-diameter non-pressurized spirally welded tubes to be used in combi-wall retaining structural systems, and reported valuable measurements on imperfection before the tests. In addition, Van Es *et al.* [5] compared test results from spiral welded pipes with the results from two longitudinally welded specimens of similar slenderness and steel grade, in order to identify the effect of the two fabrication method (spiral versus longitudinal welding) on local buckling behavior; it was reported that the spiral welded pipes exhibited similar strain capacities with the longitudinally-welded pipes for the case of rather thin-walled specimens, whereas in the case of thicker specimens (i.e values of $D/t \simeq 70$), the compressive strain capacity of spirally welded pipes was found slightly lower than that of longitudinally welded pipes.

Eltaher *et al.* [6] have used advanced finite element analysis for qualification of spiral pipes for offshore application and Zimmermann *et al.* [7] investigated the response of spiral welded pipes under strain based design. Nasim *et al.* [8] and Farouzan *et al.* [9] investigated the residual stresses of spiral welded pipes, developed by the manufacturing process. The bending deformation response of large-diameter spiral-welded tubes tested in [4] was simulated numerically by Vasilikis *et al.* [10] and a very good comparison with the test results was found; this work has also been a first attempt to account for the manufacturing process effects on structural performance in a rigorous manner. More recently, using parametric finite element analyses, Van Minnebruggen *et al.* [11] studied the influence of pipe forming angle, weld strength overmatch and material strength anisotropy on the tensile strain capacity of flawed spiral welded pipes.

The present study is part of a large project with acronym SBD-SPIPE [12], sponsored by the European Commission. The paper is aimed at examining numerically the effect of manufacturing process on the structural (buckling) performance of spiral welded pipes, used in demanding onshore applications, and in moderately deep offshore environment. The numerical simulations account for the effects of spiral cold forming process and their material behavior, with emphasis on their compressive strain capacity under bending and pressure loading conditions, extending the work presented in [13] [14].

In section 2 of the present paper, the spiral-forming process is simulated using advanced finite element models. Using the present simulation, residual stresses and material anisotropy of the line pipe at the end of the spiral manufacturing process are rigorously predicted. The subsequent section of the paper (section 3) refers to the simulation of large-scale experiments performed on spiral-welded line pipes under structural and pressure loading for the purpose of validating the numerical models. In section 4, an extensive analysis is performed to investigate the influence of spiral forming process parameters on the structural performance of spiral-welded pipes, under internally-pressurized bending conditions, and under external pressure. Finally, in section 5, a discussion of the results is offered and some basic conclusions are drawn.

2 DESCRIPTION AND NUMERICAL MODELING OF SPIRAL MANUFACTURING PROCESS

2.1 Description of spiral manufacturing process

Spiral-welded manufacturing process is a continuous process consisting of two steps: the decoiling process (first step) and the cold bending process (second step) of a hot-rolled steel coil with appropriate width and wall thickness. In the first step, the steel coil is uncoiled and becomes flat, passing through a series of rollers. Subsequently the flat strip enters a three-roller system stand is appropriately angled, where it is rolled into a circular shape in a spiral configuration (see Fig. 1). Pipe diameter is controlled by the spiral angle and the width of the plate. In most cases, just after the three-roller bending the bent pipe passes through a series of rollers around the circumference, in order to maintain its circular shape. In some cases though, these rollers do not exist, and "unloading" of the strip may occur after it passes through the three-roller bending device. Whether this "unloading" occurs or not, depends on the manufacturer's set-up, and could be an important feature in terms of its influence on mechanical response, to be examined later in the present study. Upon passing through the three-roller system, the spiral seam is welded first on the inside and then on the outside, as shown in Fig. 1. There is no special device to keep the two parts of the pipe together for welding. This is achieved by using an appropriate arrangement of the three-roller bending system. As shown in Fig. 1 the pipe is welded from inside exactly at the point where the strip exits the three-roller arrangement, this ensures that the pipe diameter remains constant during this process. After spiral forming, the spiral line pipe is cut at prescribed intervals, followed by hydrotest to verify that there exist no serious defects on the pipe weld. Moreover, an advantage of the spiral forming compared with other manufacturing process (UOE or JCOE processes) is that there is no final expansion stage. Due to the continuous nature of the forming process the circularity of the spiral pipe is very good.

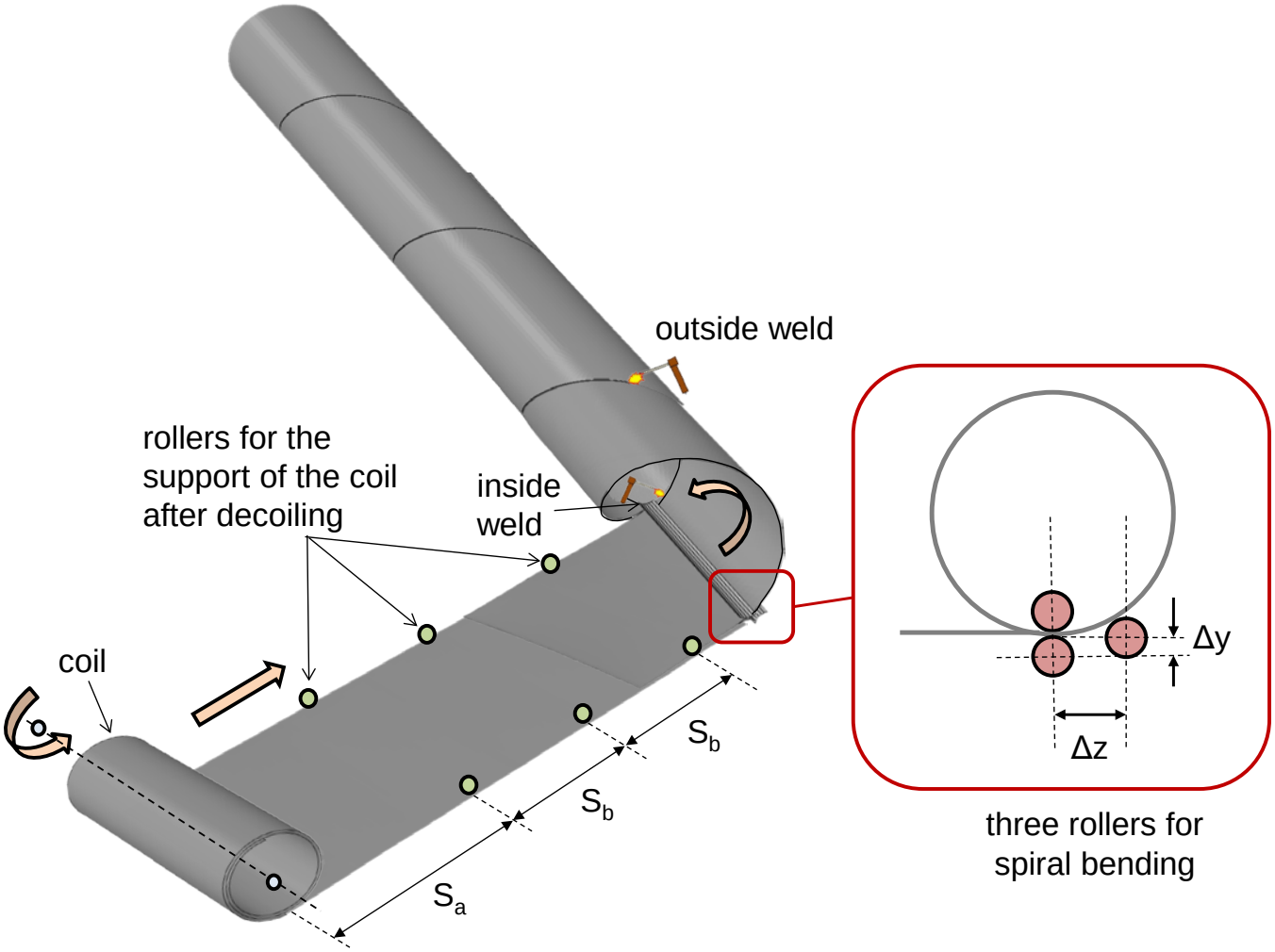

Fig. 1: Schematic representation of spiral forming processes.

2.2 Numerical modeling of cold bending process

For the simulation of the above cold bending process, numerical models are developed in the commercial finite element software ABAQUS/Standard. The steel coil is discretized using four-node, reduced-integration shell elements, referred to as S4R in ABAQUS, whereas the forming parts are modeled as rigid. Five integration points across the plate thickness were found adequate for the purpose of the present study.

Two methods are adopted for this simulation. In the first method, which is referred as "rigorous", a single numerical model is used for both decoiling and spiral bending steps. Because of hot-rolling a stress-free coil is assumed, and it is subjected to decoiling passing

through a curved rigid part, which imposes the necessary kinematic constraint as shown in Fig. 2. After decoiling, the steel strip obtains a "flat" configuration using appropriate kinematic constraints, which simulate the rollers at the edges used in the pipe mill, as shown in Fig. 1, and subsequently, in the second step it passes through a three-roller bending device, modelled with three rigid cylindrical parts. A frictionless contact interface between the coil/strip and the rigid parts is assumed. Fig. 3 depicts the numerical simulation of decoiling and spiral forming process.

To reduce the computational cost, a simplified model is also considered assuming that, in the decoiling step, the coil is subjected pure bending only. In that model, a slice with the appropriate initial curvature is used to simulate the coil, and bending is applied by controlling the rotation at the end, while keeping the other end fixed. Fig. 4 (a) depicts the numerical model of this simplified decoiling method. The residual stress and deformation state (i.e. stresses, strains, equivalent plastic strain, back stresses) obtained from this decoiling model are used as initial conditions in the second model used for simulating the spiral forming. In this model, the steel strip passes through a bending device, represented by three rigid parts, as shown in Fig. 4 (b). Despite its simplicity, this method employs two numerical models, one for decoiling and another for the forming process, which is a small disadvantage from the computational point of view. However, comparing the two methodologies for decoiling (full model and simplified) the corresponding residual stresses decoiling were found quite similar, and therefore, the simplified method will be used exclusively in the following sections of the present paper and three different initial diameters of the coil will be investigated.

The basic geometric characteristics of the numerical model for spiral bending are depicted in Fig. 3. Specifying the desired pipe diameter D, it is possible to calculate the corresponding forming (spiral) angle α and the coil width B using simple geometry, also shown in Fig. 3. In the present study, three pipes are considered. The first pipe has diameter and thickness equal to 28 in (711.19 mm) and 18 mm respectively, and is a candidate for offshore applications; the coil width B is equal to 1430 mm, which implies $\alpha = 39.8^{\circ}$. The second pipe is a 36-inch-diameter pipe (D=914.4 mm) with thickness equal to 17.1 mm, and coil width B equal to 1501

mm, so that the value of α is equal to 31.2° and is a candidate for onshore applications. The third pipe has a diameter equal to 48-inches (D=1219.19 mm), thickness equal to 19.3 mm, coil width B equal to 1759.7 mm and a spiral angel α equal to 27.35°; it is also a candidate for onshore applications. The above information, as well as the distances between the rollers in the straightened part and those in the three-roller arrangement are shown in Fig. 1, and in Table 1.

Throughout the forming process (decoiling, spiral forming) all material parameters (stresses, strains) are recorded, and their final values (including pipe hydrotest to be described in detail in the next section) are used as initial stress/strain conditions for the finite element models employed for simulating the structural performance of the pipes described in detail in sections 3 and 4. Note that hydrotest is an essential part of the linepipe production process at the pipe mill, and ensures that serious weld flaws are detected and pressure containment is maintained. In the present analysis, the level of hydrotest pressure is assumed equal to 90% of yield pressure ($0.9P_y$), a typical value used in the pipe mill. In addition, it influences the residual stress and deformation state and its effect on structural performance of the pipe will be presented in a subsequent paragraph.

Another feature of the manufacturing process is whether "unloading" of the strip is allowed or not, after it passes through the three-roller bending device, shown schematically in Fig. 5. Two cases are examined: (1) the case where unloading is restricted denoted as "NU" using a series of rollers around the circumference just after the steel strip passes through the three-roller system and (2), the case where "unloading" is allowed denoted as "U". Case "NU" (Fig. 5a) is most likely to occur in pipemills for spiral pipe fabrication, but Case "U" (Fig. 5b) is also examined for the sake of completeness. Fig. 6 illustrates schematically the stress-strain response during decoiling and spiral bending for both cases. In the "NU" case the stresses are represented by the "NU" location on the stress strain path in Fig. 6, while in the U case the corresponding stresses are considerable lower due to stress release.

Table 1: Details of manufacturing process.

	D (mm)	t (mm)	α (degrees)	B (mm)	Δy (mm)	Δz (mm)	S_a (mm)	S_b (mm)
Pipe I	711.19	18	39.8	1430	101	141	1500	1000
Pipe II	914.4	17.1	31.2	1501	90.1	192	1500	1000
Pipe III	1219.19	19.3	27.35	1759.7	118.65	192.36	1500	1000

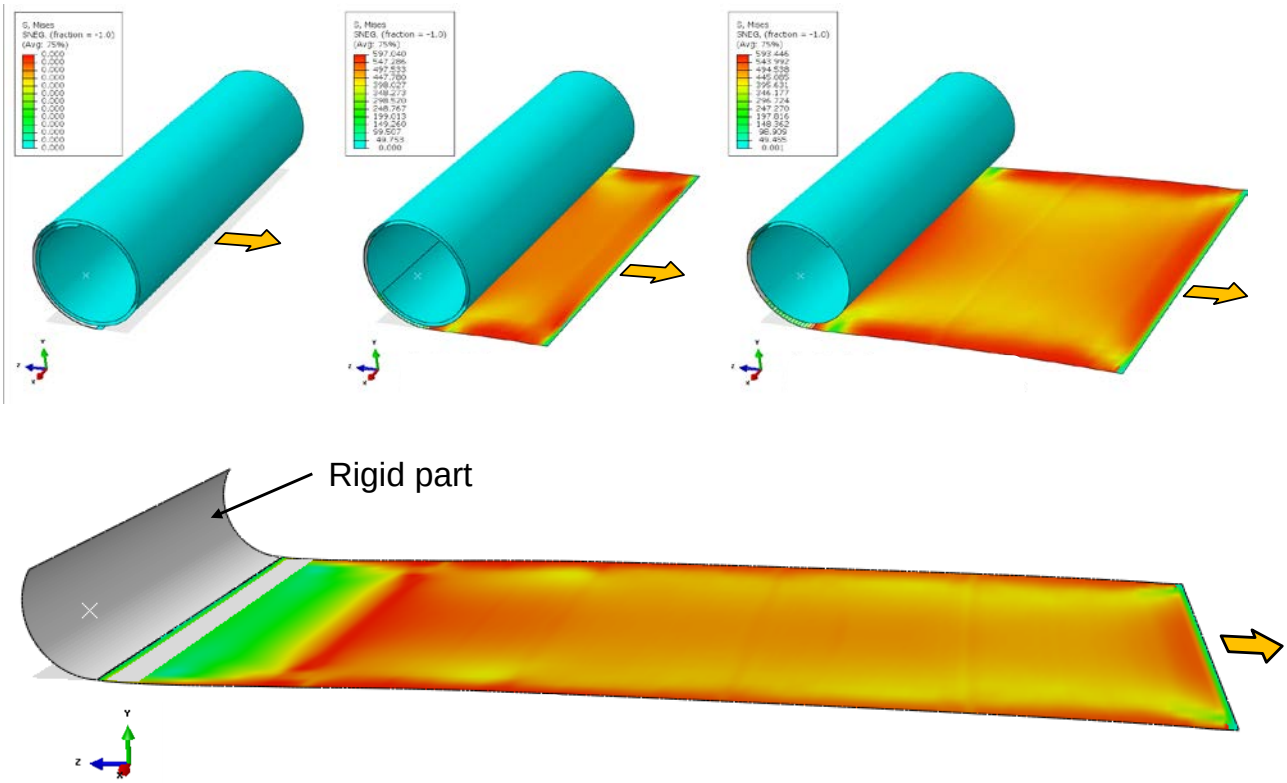

Fig. 2: Numerical simulation of decoiling and straightening process.

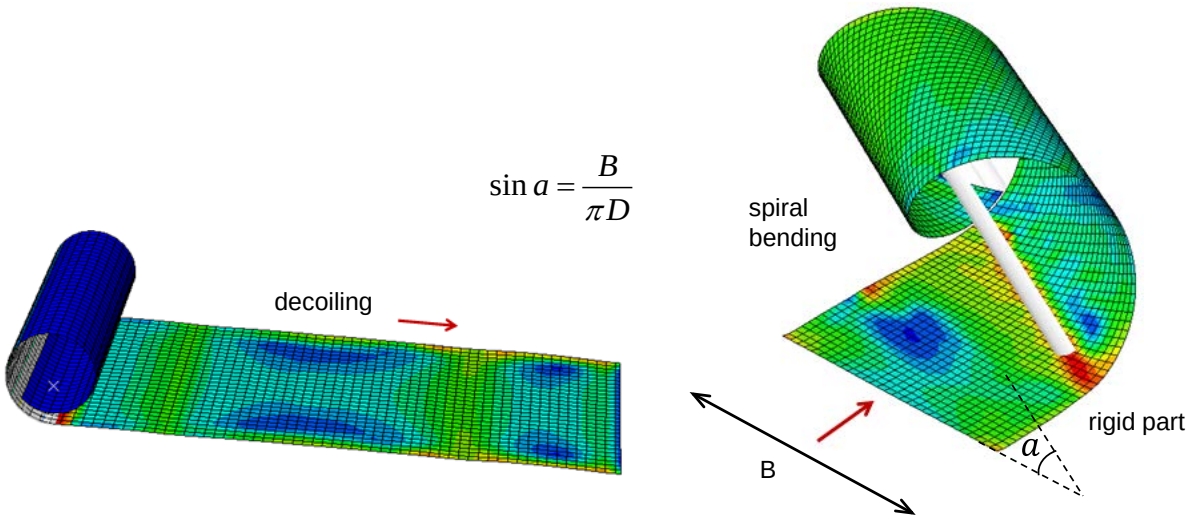

(a) (b)

Fig. 3: Numerical simulation of spiral forming; (a) decoiling and (b) spiral bending process.

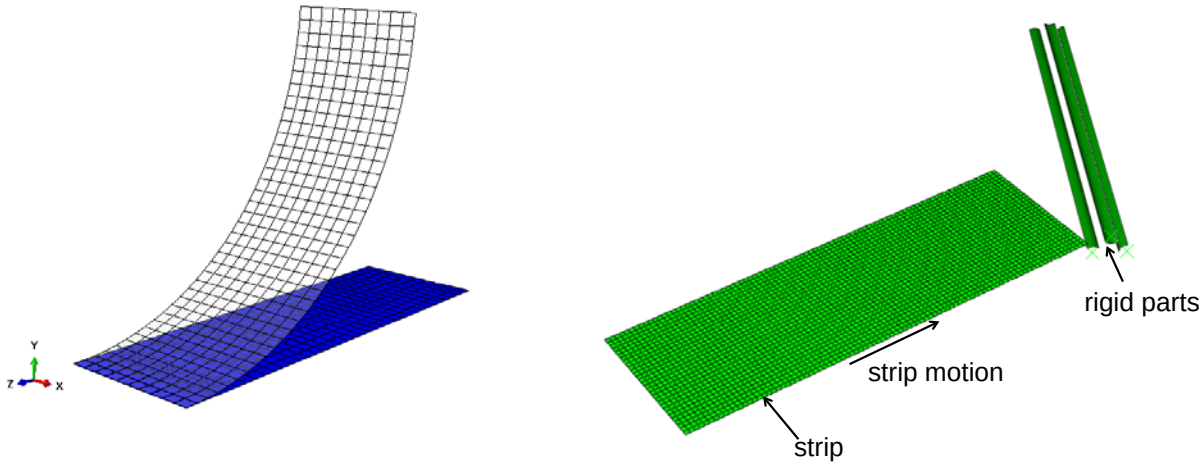

(a) (b)

Fig. 4: (a) Simplified method for simulating decoiling; (b) Numerical simulation of spiral forming in the simplified methodology.

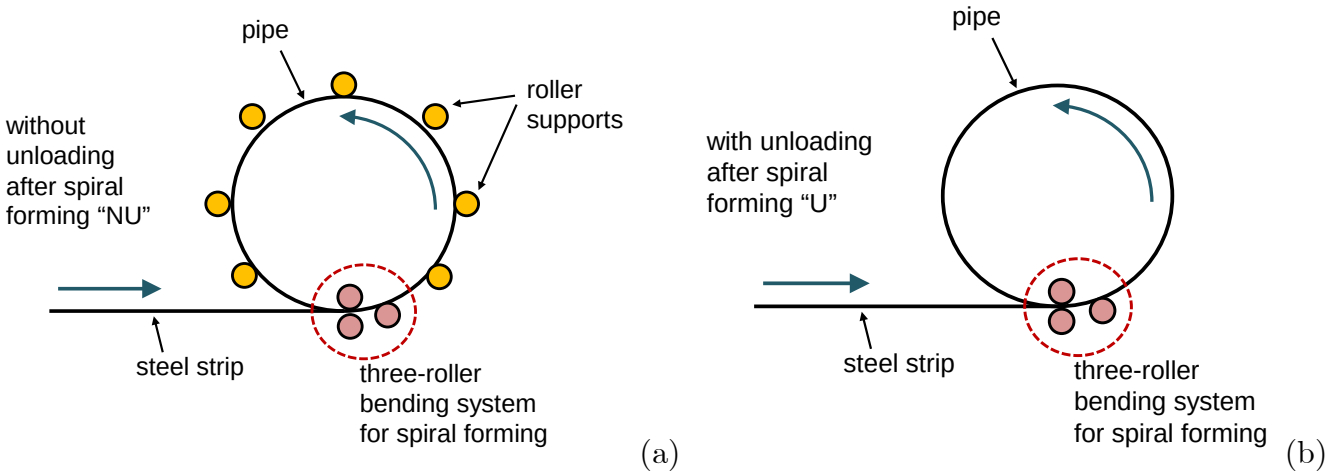

Fig. 5: Schematic representation of spiral forming without (a) and with (b) “unloading” after passing from the three-roller system (“NU” and “U” cases).

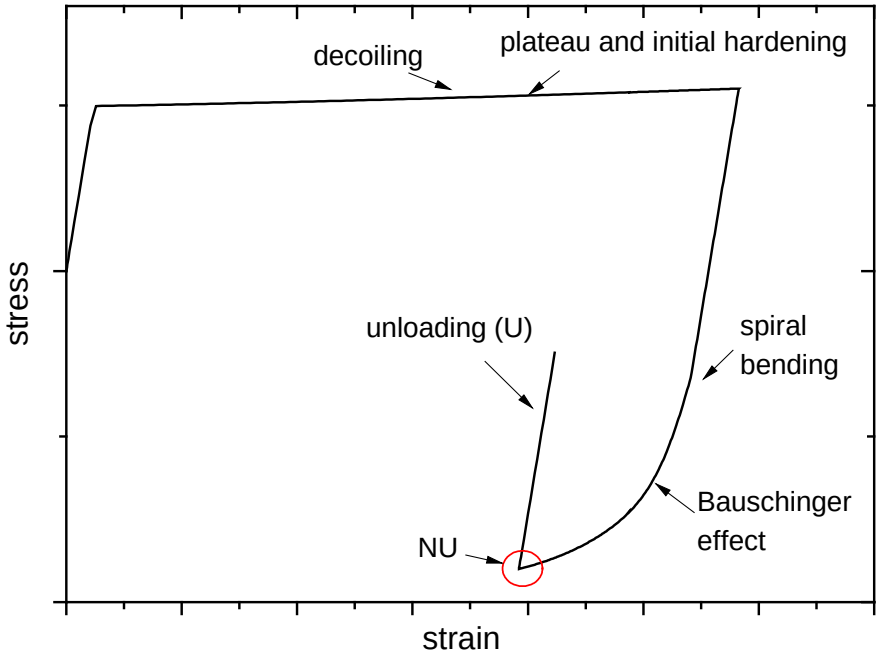

Fig. 6: Schematic representation of stress-strain response during decoiling and spiral forming process.

2.3 Constitutive modeling

The simulation of material behavior under reverse (cyclic) loading conditions is of major importance for reliable modeling of the spiral forming process and prediction of pipe ultimate capacity. During decoiling and spiral forming, the steel material behavior is characterized by two main features: (a) the yield plateau of the stress-strain curve upon initial yielding, (b) the Bauschinger effect under reverse plastic loading. Both features are taken into account in the constitutive material model. The model and its implementation are presented briefly below.

2.3.1 Model formulation

The constitutive model is an extension of the one proposed in [15] for cyclic plasticity. It considers von Mises yield surface:

$$F = \frac{1}{2}(\mathbf{s}-\mathbf{a})\cdot(\mathbf{s}-\mathbf{a}) - \frac{k^2}{3} = 0 \tag{1}$$

where $\mathbf{s}$ is the deviatoric stress tensor, $\mathbf{a}$ is the back stress tensor, and k is the size of the yield surface, expressed as a function of the equivalent plastic strain ε_q:

$$k(\varepsilon_q) = \sigma_Y + Q(1-e^{-b\varepsilon_q}) \tag{2}$$

In the above expression, σ_Y is the initial value of uniaxial yield stress, Q and b are hardening parameters, and ε_q is the time integral of the equivalent plastic strain rate $\dot{\varepsilon}_q$, defined in terms of the plastic strain rate tensor $\dot{\boldsymbol{\varepsilon}}^P$ as follows:

$$\dot{\varepsilon}_q = \sqrt{\frac{2}{3}\dot{\boldsymbol{\varepsilon}}^P \cdot \dot{\boldsymbol{\varepsilon}}^P} \tag{3}$$

The kinematic hardening rule for the back stress tensor rate is adopted

$$\dot{\mathbf{a}} = C\dot{\boldsymbol{\varepsilon}}^p - \gamma \mathbf{a}\dot{\varepsilon}_q \tag{4}$$

where $\dot{\boldsymbol{\varepsilon}}^p$ is the plastic strain rate tensor, and C, γ are parameters calibrated from cyclic test data. In the present model, to account for the smooth transition from elastic to plastic response, as indicated by the Bauschinger effect, $C = C(\varepsilon'_q)$ is assumed to be a function of equivalent plastic strain ε'_q accumulated at each plastic loading step:

$$C(\varepsilon'_q) = C_0 + Q_b(1-e^{-c\varepsilon'_q}) \tag{5}$$

where C_0 is the initial value of C at first yielding, whereas Q_b and c are hardening parameters. Furthermore, to describe the yield plateau at initial yielding, a critical strain level ε_{ql} is defined, as the point where the plastic plateau region ends, following the proposal of Ucak and Tsopelas [16]. If the computed equivalent plastic strain is less than the value of ε_{ql}, a very small value of the hardening parameter C is assumed, corresponding to plastic plateau. When this critical value ε_{ql} is exceeded or when reverse plastic loading occurs, C becomes the function of the equivalent plastic strain ε_q' expressed by equation (5), representing strain hardening and the Bauschinger effect.

Finally, an associative flow rule is employed, and using equation (6):

$$\dot{\boldsymbol{\varepsilon}}^p = \frac{3}{2k(\varepsilon_q)} \dot{\varepsilon}_q (\mathbf{s} - \mathbf{a}) \tag{6}$$

and the rate of stress is related to the rate of elastic strain as follows

$$\dot{\boldsymbol{\sigma}} = \mathbf{D}\,(\dot{\boldsymbol{\varepsilon}} - \dot{\boldsymbol{\varepsilon}}^P) \tag{7}$$

where $\mathbf{D}$ is the fourth-order elastic rigidity tensor.

2.3.2 Numerical implementation of constitutive model

The numerical implementation of the above model follows an Euler-backward "elastic predictor – plastic corrector" scheme. Given the state parameters $(\mathbf{s}_n, \mathbf{a}_n, \varepsilon_{qn})$ at state n and for a given strain increment $\Delta\boldsymbol{\varepsilon}$, the new state parameters at n+1 $(\mathbf{s}_{n+1}, \mathbf{a}_{n+1}, \varepsilon_{qn+1})$ are calculated as described below. More specifically, integration of (7) and (6) results in

$$\boldsymbol{\sigma}_{n+1} = \boldsymbol{\sigma}^{(e)} - 2G\Delta\boldsymbol{\varepsilon}^p \tag{8}$$

$$\Delta\boldsymbol{\varepsilon}^p = \frac{3}{2k(\varepsilon_{qn+1})} \Delta\varepsilon_q (\mathbf{s}_{n+1} - \mathbf{a}_{n+1}), \tag{9}$$

where $\Delta(\cdot)$ is the increment of $(\cdot)$ from state n to state n+1, $\Delta\varepsilon_q$ is obtained integrating (3),

$$\boldsymbol{\sigma}^{(e)} = \boldsymbol{\sigma}_n + \mathbf{D}\Delta\boldsymbol{\varepsilon} \tag{10}$$

is the elastic trial stress, and

$$\Delta\boldsymbol{\varepsilon}_q = \sqrt{\frac{2}{3}\Delta\boldsymbol{\varepsilon}^p \cdot \Delta\boldsymbol{\varepsilon}^p} \tag{11}$$

Furthermore, integration of the back-stress evolution equation (4) results in

$$\mathbf{a}_{n+1} = \mathbf{a}_n + C(\varepsilon'_{q+1})\Delta\boldsymbol{\varepsilon}^p - \gamma\mathbf{a}_{n+1}\Delta\varepsilon_q \tag{12}$$

Enforcing the consistency condition at the final state n+1, and using equations (2), (8), (9), and (12) one results in the following equation in terms of $\Delta\varepsilon_q$

$$\frac{1}{B^2}\left(\mathbf{s}^{(e)} - \frac{1}{1+\gamma\Delta\varepsilon_q}\mathbf{a}_n\right)\cdot\left(\mathbf{s}^{(e)} - \frac{1}{1+\gamma\Delta\varepsilon_q}\mathbf{a}_n\right) - \frac{2}{3}k^2(\varepsilon_{qn+1}) = 0 \tag{13}$$

where

$$B = 1 + \frac{3}{k(\varepsilon_{qn+1})}\left(G + \frac{C(\varepsilon'_{q+1})}{2(1+\gamma\Delta\varepsilon_q)}\right)\Delta\varepsilon_q \tag{14}$$

and $\mathbf{s}^{(e)}$ is the deviatoric part of trial stress $\boldsymbol{\sigma}^{(e)}$. Equation (13) is solved through an iterative Newton–Raphson scheme.

The elastic-plastic model is implemented in a user material subroutine (UMAT) in ABAQUS/Standard. In the present study, cyclic tests from a steel coil of X70 grade are employed (Fig. 7), provided by Onderzoekscentrum Voor Aanwending Van Staal N.V (OCAS) [12]. Material specimens (steel strips) extracted from different directions of steel coil of X70 grade indicated that the initial anisotropy of the coil material is negligible and, therefore, it is not taken into account.

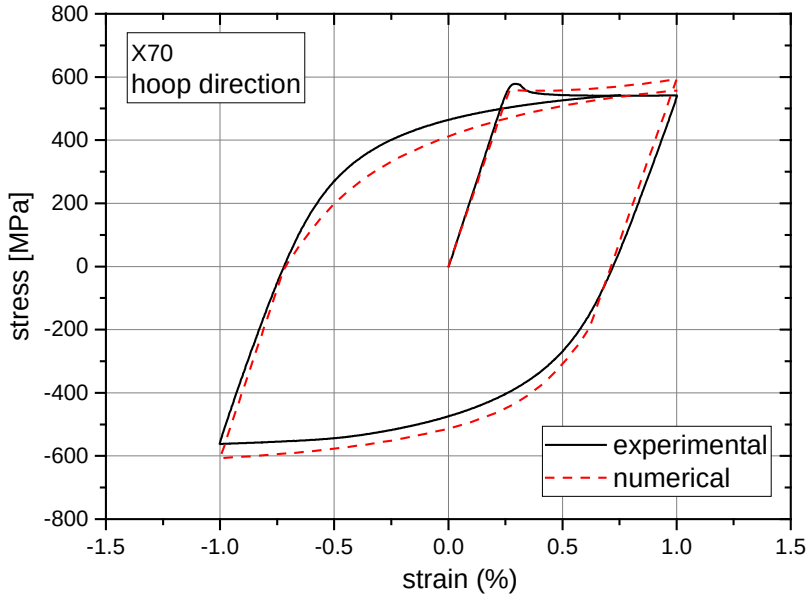

Fig. 7: Stress-strain curve from X70 grade steel coil; curve provided by OCAS [12].

2.4 Numerical results for spiral manufacturing process

During the spiral cold bending forming process the material enters well into the strain hardening region, so that significant stresses and deformations develop. In the present analysis the effect of coil diameter, the existence of "unloading" and the effect of hydrotesting are examined. Three values of coil diameter are considered: 0.5m (representing the inner part of coil), 1m (an intermediate value) and 2m (representing the outer part of coil). The above minimum and maximum values are representative values for steel coils widely used in spiral pipe production. As coil diameter decreases, coil deformation after flattening (de-coiling) increases. Fig. 8 depicts the stress-strain response of a point located at the inner surface of the coil during decoiling and (flattening), whereas the arrows indicate the level of stress and strain of the strip in the flat configuration.

The contour plots depicted in Fig. 9 and Fig. 10 refer to the spiral forming of 36-inch-diameter pipe for the "U" and "NU" cases and D_c equal to 2m, at the outer part of the coil. The results show, that this "unloading" after passing through the three-roller system (spiral bending) may have a significant effect on the stress state of the formed pipe and, therefore, it is expected to influence its structural performance. The influence of hydrotest is mainly the change of residual stresses and generally the change of stress-strain response of the pipe due to the forming process and it will be discussed extensively in the following sections. The influence of the above parameters is examined in the next sections, in terms of their effect on (a) four-point bending response under internal pressure, and (b) external pressure capacity.

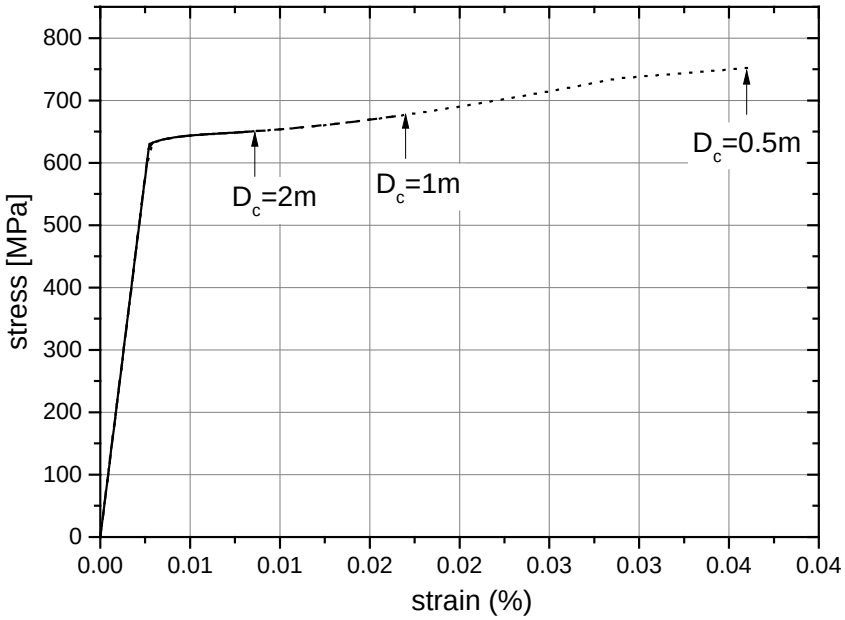

Fig. 8: Stress-strain response during decoiling for the three different coil diameter values (D_c).

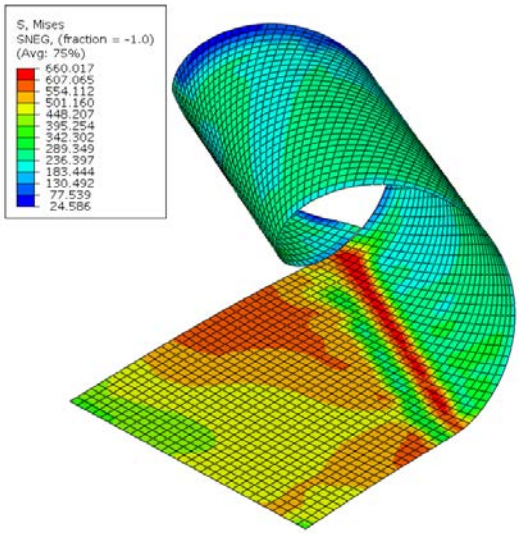

Fig. 9: Distribution of Von Mises stresses (inner surface) during spiral cold forming with "unloading" ("U" case).

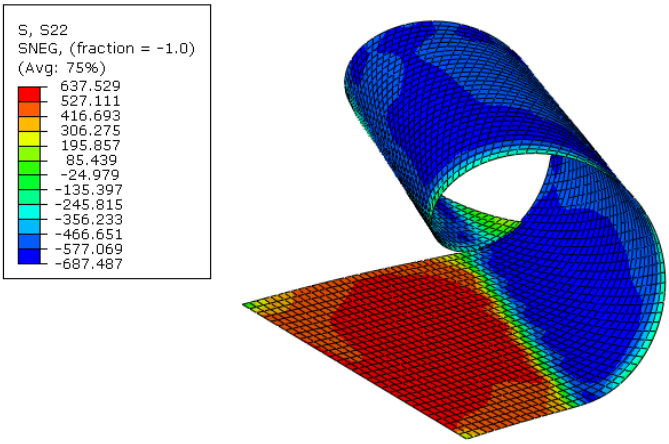

Fig. 10: Distribution of Von Mises stresses (inner surface) during spiral cold forming without "unloading" ("NU" case).

Consequently, the stress–strain response of the steel is affected and the final material is characterized by anisotropy. In practice, material anisotropy at the end of the spiral forming process is measured by extracting two strip specimens, one strip in the longitudinal and a second strip in the hoop direction of the line pipe, and performing uniaxial tension tests, so that the corresponding stress-strain curves in each direction are obtained.

A numerical simulation of the above practical procedure is attempted in the present study, also performed for UOE pipes in [17] [18]. Throughout the simulation of the forming process all material parameters (i.e. stresses, strains, equivalent plastic strain, back stresses) are recorded. Subsequently, a "unit cube" finite element model is considered, and the material parameters at a representative location on the outer surface of the pipe after the entire manufacturing process, away from the spiral weld, are introduced as initial state of this "unit cube" model. An analysis step with zero external loading is performed first on this model, simulating the extraction of the strip specimen from the pipe; at this first step, the residual stresses are released but plastic deformations due to the forming process are maintained. Subsequently, a second step is performed where the "unit cube" is loaded under uniaxial tension in the hoop or the axial direction. The response of the unit cube provides the mechanical behavior of pipe material at this specific direction of loading. Considering the tensile stress-strain curve in the

axial direction of the pipe as the fundamental response of the material, the different behavior in the hoop direction is quantified in terms of the following anisotropy parameter:

$$S = \frac{\sigma_{Y\theta}}{\sigma_{Yx}} \tag{15}$$

where σ_{Yx} is the tensile yield stress in the pipe axial direction and $\sigma_{Y\theta}$ is the circumferential yield stress of pipe material.

Representative results for the anisotropy of the 36-inch-diameter pipe are shown in Fig. 11, in terms of the stress-strain response. The solid curves, denoted as "experimental", are obtained from testing real strip specimens, extracted from the pipe under consideration, as reported by Salzgitter Mannesmann Forschung GmbH (SZMF) [12]. In Fig. 11, the numerical predictions are compared with these test results, and the comparison shows good agreement in terms of the yield stress. In those calculations, the initial coil diameter is considered equal to 1m and unloading is restricted ("NU"). The value of anisotropy parameter S of the pipe after the forming process and hydrotest is equal to 0.912. The difference in hardening is attributed to the fact that no information has been available for the coil material, used for manufacturing the pipes under consideration. The analysis considers the coil material properties shown in Fig. 7, but this coil does not correspond to the pipe considered in Fig. 11.

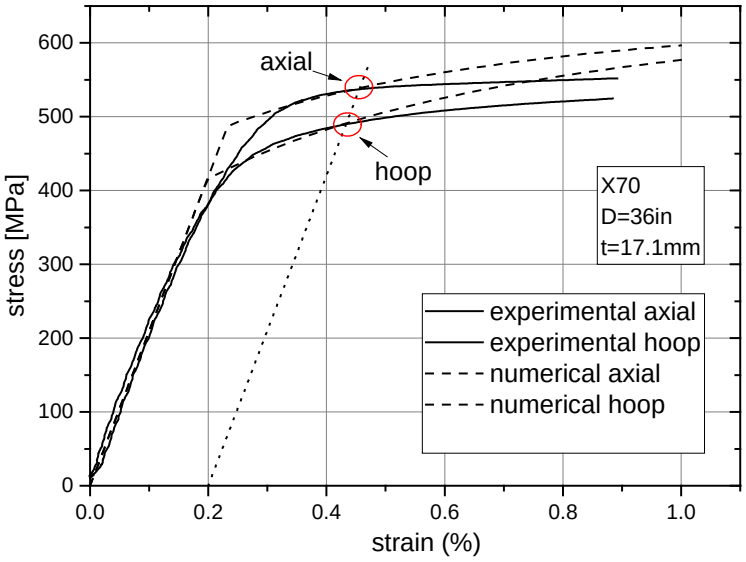

Fig. 11: Comparison of axial and circumferential tensile response from experiments and numerical results.

3 FINITE ELEMENT SIMULATION OF PIPE EXPERIMENTAL TESTING

Experimental results from four spiral welded pipes are considered, made of X70 steel material. Two pipes have been provided by Mannesmann Grossrohr GmbH. The first pipe is candidate for onshore applications, while the second pipe can be used in shallow water offshore applications. The other two pipes have been provided by Corinth Pipeworks S.A. (CPW), and are also typical for onshore applications. The corresponding experiments have been performed in the course of the SBD-SPIPE project [12] and consist of a collapse test and three four-point bending tests. These tests are simulated in order to compare the experimental results with the numerical predictions, for the purpose of validating the numerical models. Based on appropriate measurements made on the pipe specimens [12], geometric imperfections are used in the initial pipe configuration.

For simulating structural performance of the spiral welded pipes under four-point bending or external pressure, numerical models are developed as shown in Fig. 12, Fig. 13 and Fig. 14. An appropriate helical partition is considered in order to develop a spiral mesh that follows the spiral weld configuration of Fig. 12, which allows for considering the overmatching properties of the weld material. The pipe is discretized using four-node, reduced-integration shell finite elements, referred to as S4R in ABAQUS.

As mentioned in the previous section, hydrotest is simulated. Despite the fact that the hydrotest is the last step of the manufacturing process, in our case, for computational convenience, it is not part of the spiral forming model but it is the first step in the model used for structural performance. After the hydrotest step, the structural analysis of the spiral welded pipe is performed under bending and/or pressure. In the case of pure external pressure loading, pressure is gradually applied, using Riks' continuation algorithm, until the collapse pressure of the pipe is reached, so that the post-buckling path and the corresponding configuration are both obtained. In the case of internally-pressurized bending (four-point bending), internal pressure is applied first up to the desired level and, subsequently, keeping the pressure level constant, bending deformation is gradually increased. Displacement in a four point bending scheme is applied, to obtain local buckling failure and post buckling response.

In the present section, using the numerical tools described above, a simulation analysis of experiments, conducted in the framework of SBD-SPIPE project, is performed for the purpose of validating the numerical models, to be used for the parametric study in the subsequent section. The tests under consideration are (a) one collapse test and (b) three bending tests. Given the fact that information for the steel coil material of the tested pipes is not available, the following methodology had been adopted for simulating the experiments: (a) the forming process of the pipe is simulated first using the UMAT model and the material curve of Fig. 7 as an initial stress-strain material curve for the X70 steel coil material; (b) the final state (stress, strains, equivalent plastic strain, back stress) from this forming analysis is inserted as initial state in the structural model, (c) the structural analysis of the pipe is performed using an isotropic hardening plasticity model with the stress-strain curve available for the pipe under consideration obtained from uniaxial testing. These stress-strain curves for the three tested pipes are shown in Fig. 15. Preliminary calculations with overmatching properties of the weld material indicated an insignificant effect of overmatching on the structural response, and therefore, this feature has been neglected in the present study. In section 3.1, the response of a relatively thick spiral-welded pipe is examined subjected to external pressure, whereas in section 3.2, the three internally-pressurized bending tests of the 36-inch-diameter and 48-inch-diameter pipes are simulated.

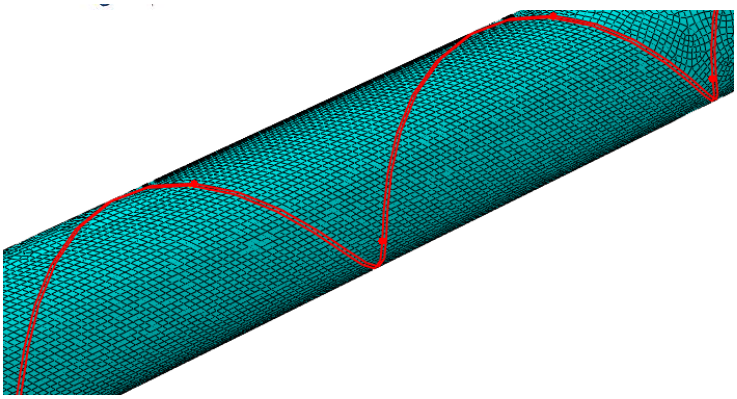

Fig. 12: Finite element model in ABAQUS/Standard detail of spiral mesh of shell elements.

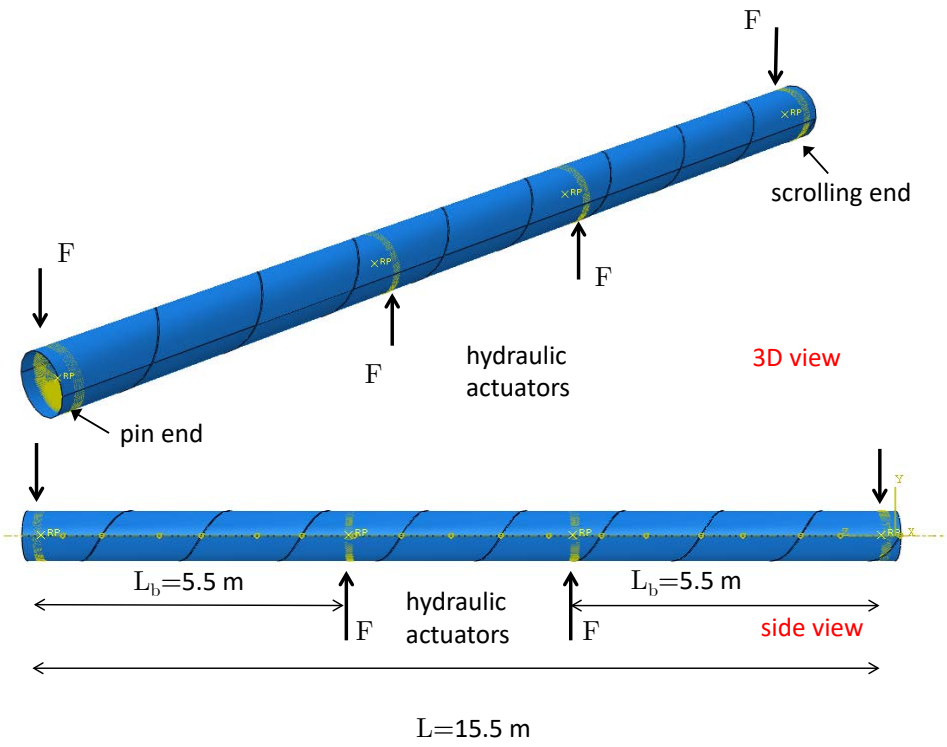

Fig. 13: Finite element model in ABAQUS/Standard for simulating the SZMF four-point bending tests.

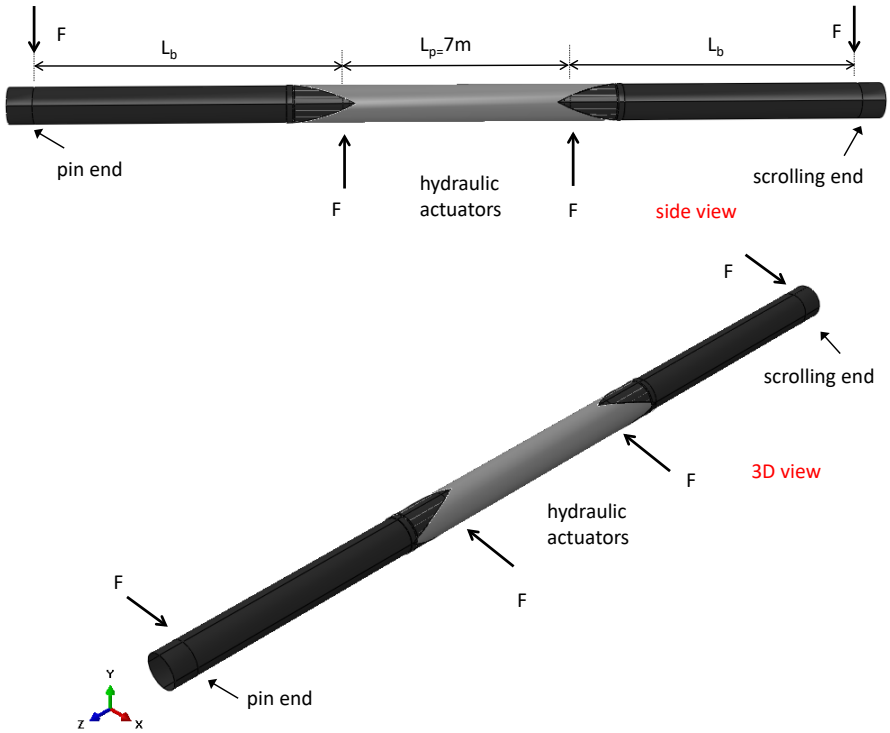

Fig. 14: Numerical finite element model in ABAQUS/Standard for simulating the CSM four-point bending set-up.

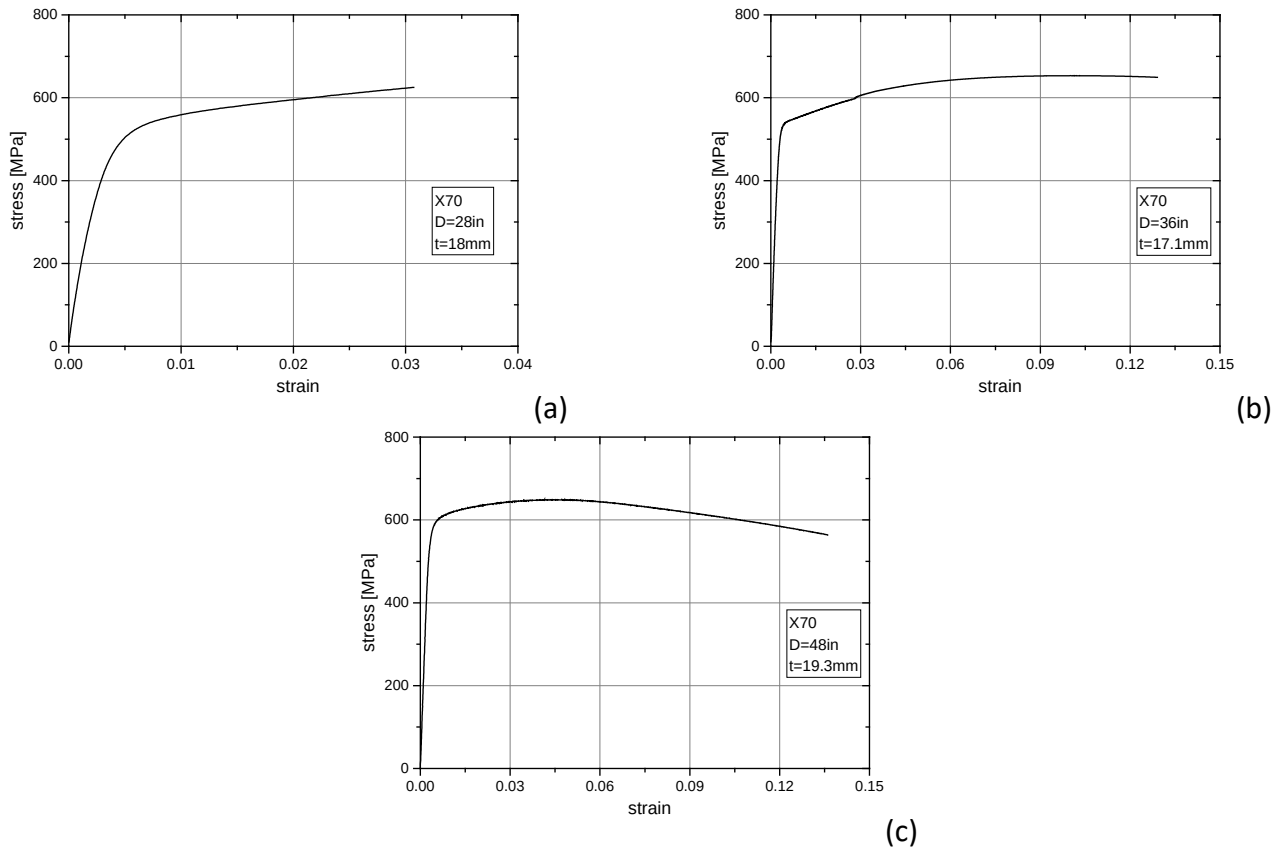

Fig. 15: Compressive hoop stress-strain curve from the 28-inch-diameter spiral pipe (a) and tensile axial stress-strain curve from the 36-inch (b) and 48-inch- diameter spiral pipes (c).

3.1 Simulation of external pressure (collapse) test

The pipe diameter is equal to 28 inches, the thickness is 18mm, the material grade is X70 as referred above and the length of the pipe is 6m. Pipe initial ovalization has also been measured before testing. Herein, it is defined as the ratio $\left(D_{\max}-D_{\min}\right)/\left(D_{\max}+D_{\min}\right)$, and constitutes a major geometric imperfection parameter in offshore pipeline design. The measurements indicated a value of initial ovalization equal to 0.05%, which is well below the allowable value in relevant design standards [20]. The collapse pressure i.e. the maximum pressure sustained by specimen during the test is equal to 7.69 MPa. Using the numerical model the collapse pressure prediction is 7.66 MPa, showing an excellent agreement. Fig. 16 shows the deformed (collapsed) shape of the pipe under external pressure in an oval configuration, obtained numerically.

3.2 Simulation of four-point bending tests

Three four-point bending tests are also simulated. The first test, conducted by SZMF (Test 1), has been performed under internal pressure equal to $0.72P_y$ (where P_y is the nominal yield pressure, equal to $2\sigma_y t/\mathrm{D}$). The other two tests have been performed by CSM; in one test, the pipe has not been pressurized (Test 2), whereas, in the other test, internal pressure has been equal to $0.72P_y$ (Test 3). The set-up of the experiments is presented in Fig. 13 and Fig. 14 respectively. The pipe of Test 1 has diameter equal to 36 inches, average thickness equal to 17.5mm, measured before testing, and the steel material grade is X70. The value of initial wrinkling amplitude was measured equal to 1%. The structural length of the pipe is 15.5m and the actuators are located at length L_b equal to 5.5m from the end supports. Fig. 13 depicts the numerical model and the position of the actuators and internal supports. The two 48-inch diameter specimens have average thickness 19.3 mm and material grade X70. The value of initial wrinkling amplitude was measured equal to 4%. For the non-pressurized specimen Test 2 the structural length of the pipe is equal to 28.6m and the actuators are located at a distance $\mathrm{L_b}$ equal to 10.8m from the end supports. For the internally-pressurized specimen Test 3 the structural length of the pipe is equal to 27m and the actuators are located at a distance of 10m from the end supports. In all three pipes, a wrinkling imperfection is considered in their initial pipe geometry, in the form of the first buckling mode, obtained through a standard eigenvalue analysis of the bent tube. Based on measurements before testing, the amplitude of this wrinkling is equal to 1% for specimen 1, and 4% for the other two specimens.

Fig. 14 depicts the numerical model, the position of the actuators and the locations of supports. The experimental results in terms of force-displacement are shown in Fig. 17, Fig. 18 and Fig. 19. In all cases, the comparison indicates very good agreement. Moreover, the deformed shape of the pipes shown in Fig. 20, Fig. 21 and Fig. 22 respectively are characterized by pipe wall bulging at the buckled area, a typical pattern for internally pressurized pipes subjected to bending [21], [22]. The results indicate a very good agreement of the buckled configurations obtained numerically with the shape of the buckled specimens. The buckled shape of Test 1 is characterized by a bulging pattern at the vicinity of load application locations, also observed in the experiments. In Test 2 a buckle occurred at the middle of the

pipe, whereas in Test 3 two buckles occurred at a distance from the location of load application.

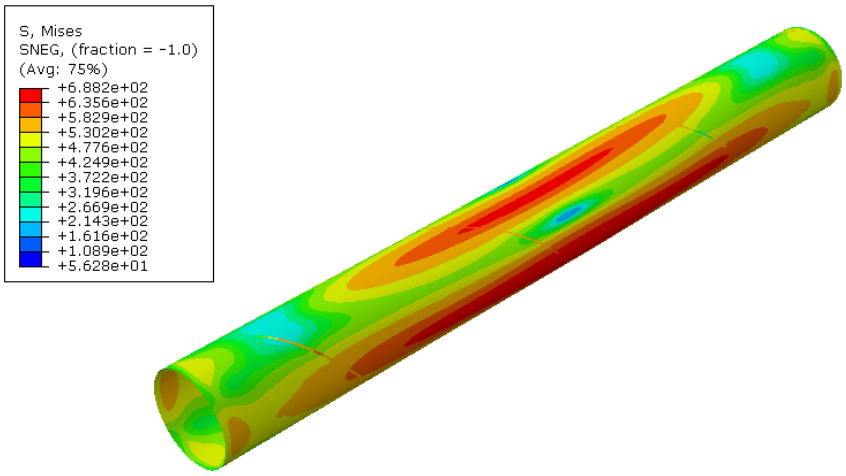

Fig. 16: Deformed shape of the 28-inch-diameter spiral pipe due to external pressure collapse; post-buckling oval configuration.

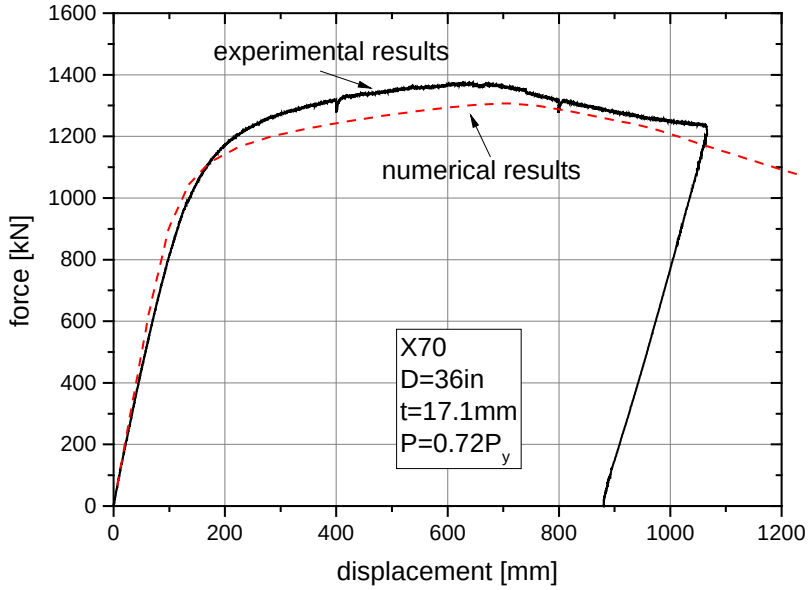

Fig. 17: Comparison of experimental and numerical results for the four-point bending test performed by SZMF (Test 1).

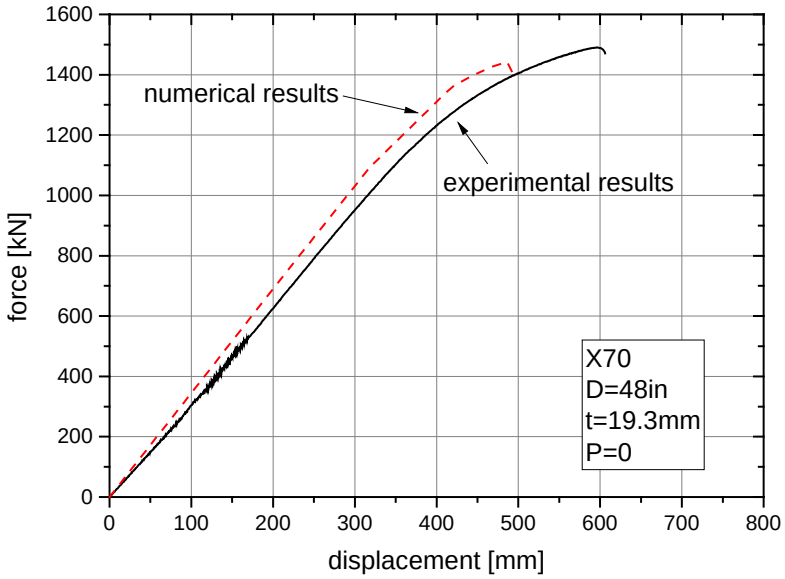

Fig. 18: Comparison of experimental and numerical results for the non-pressurized 48-inch four-point bending test on 48 inch-diameter pipe (Test 2).

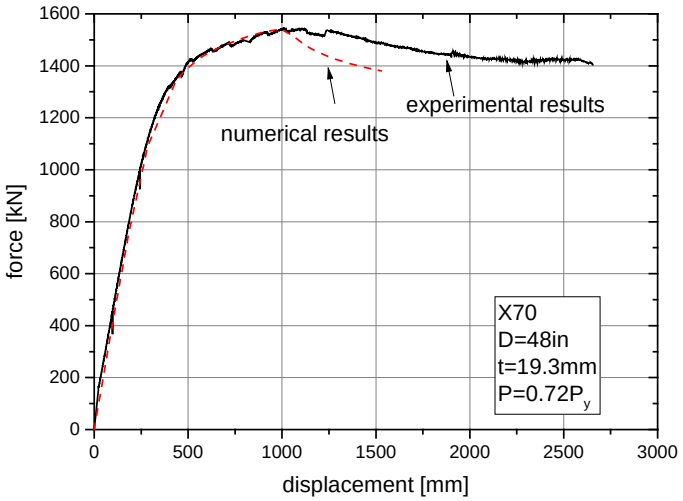

Fig. 19: Comparison of experimental and numerical results for the pressurized 48-inch four-point bending test on 48 inch-diameter pipe (Test 3).

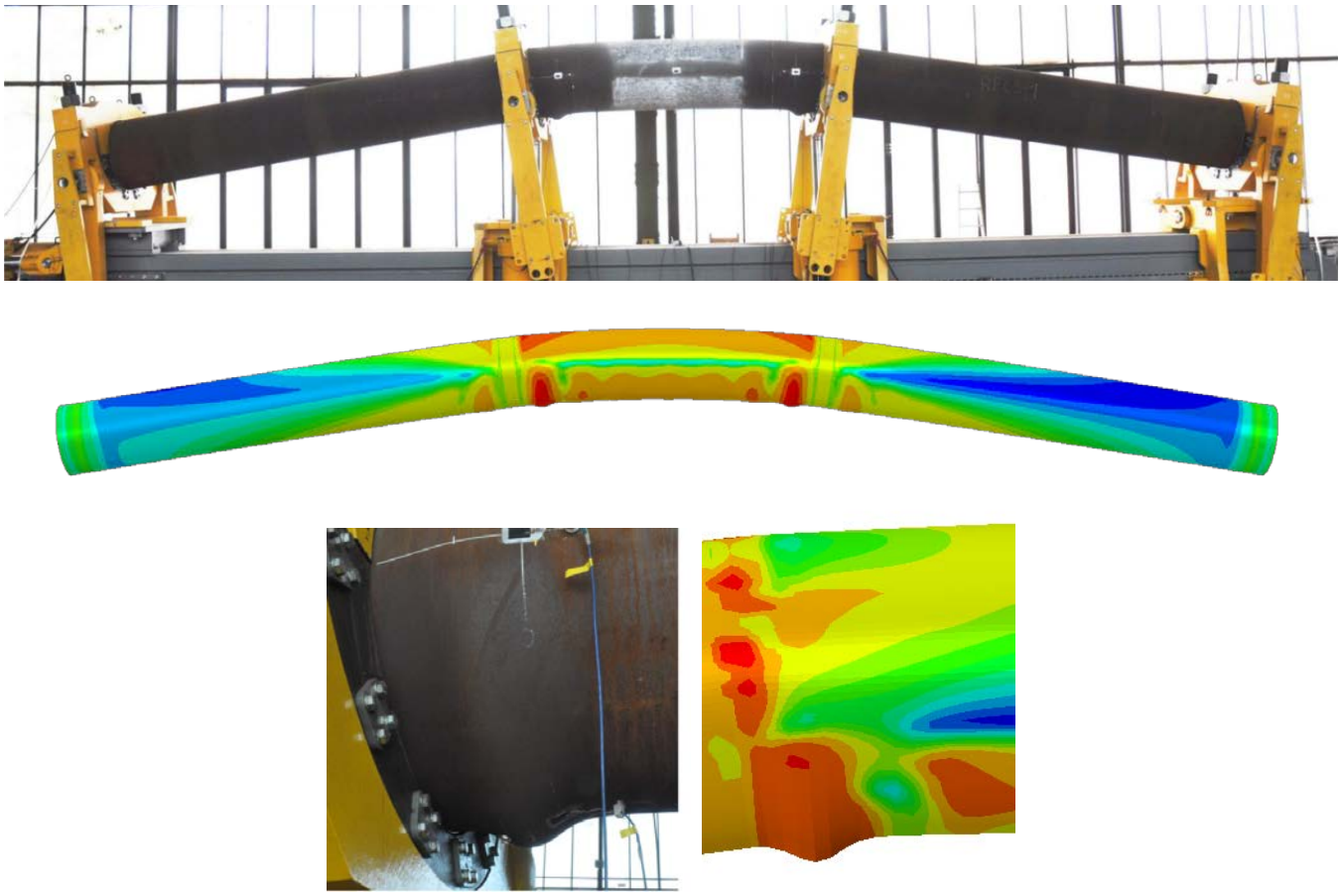

Fig. 20: Deformed shapes for the 36-inch, pressurized-bending test (numerical versus experiments); buckle occurred at the vicinity of the internal support (Test 1).

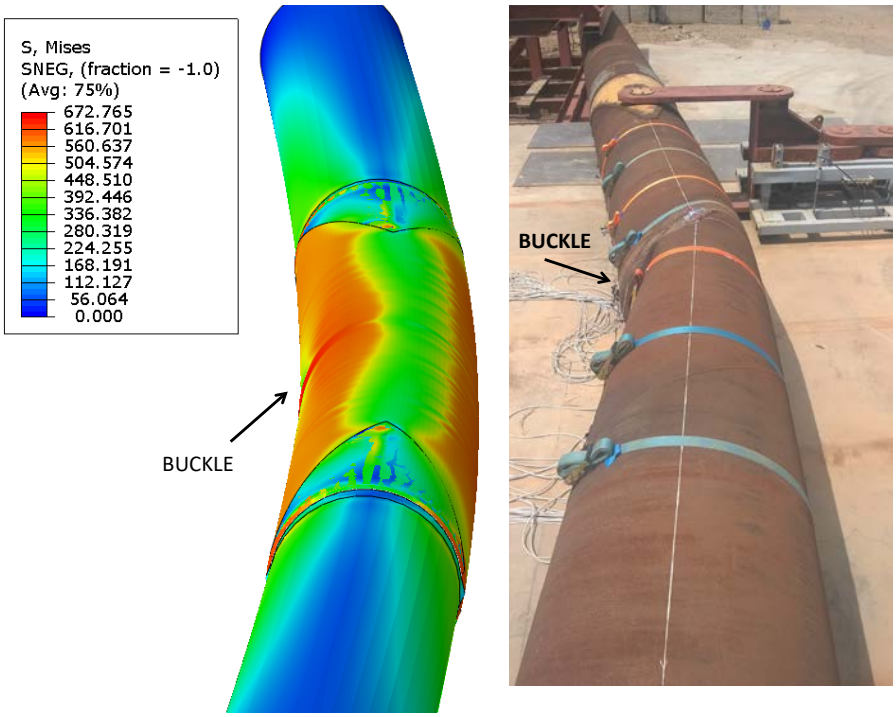

Fig. 21: Deformed (buckled) shapes (numerical versus experimental) for the non-pressurized 48-inch four-point bending test on 48 inch-diameter pipe (Test 2).

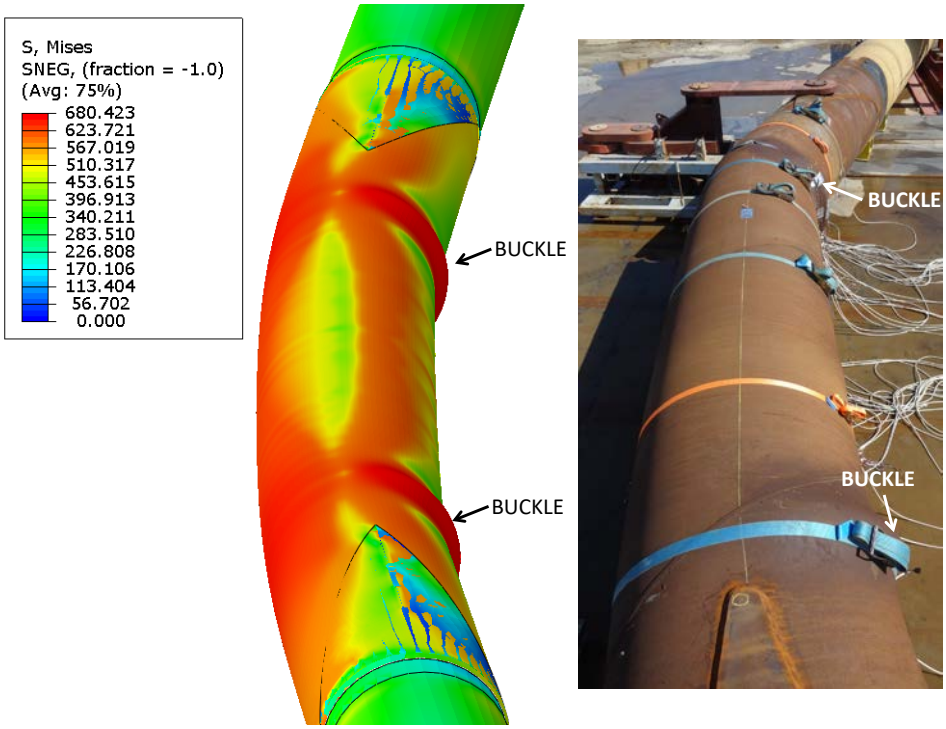

Fig. 22: Deformed (buckled) shapes (numerical versus experimental) for the pressurized 48-inch four-point bending test on 48 inch-diameter pipe (Test 3).

4 NUMERICAL SIMULATION OF THE STRUCTURAL BEHAVIOR OF SPIRAL PIPES

Following the simulation of the forming process and the validation of the numerical structural models through experimental data, the spiral pipes under consideration are subjected to loading conditions, referring to demanding pipeline applications. Motivated by ground-induced actions in geohazerd areas, paragraph 4.1 examines the effect of spiral cold bending process on bending capacity in the presence of internal pressure. Furthermore, in paragraph 4.2, the effect of spiral cold bending process on the ultimate capacity of spiral pipes is presented.

In the present study, the effect of three parameters from the manufacturing process on structural performance are examined, namely (a) the effect of coil diameter D_c (b) whether "unloading" or not occurs after the spiral three-roller bending process, and (c) the effect of hydrotest. In the following, if "unloading" is allowed, the case is denoted as "U", whereas, if unloading is restrained, it is denoted as "NU". Finally the application of hydrotest on a pipe or not is denoted as "H" or "NH" respectively. The residual stress state computed from spiral forming are used as initial condition in the structural performance model. In all cases analyzed, the in-house material model (UMAT) is employed, for both the manufacturing model and the structural model; the output of the former is used as input for the latter. Furthermore, the X70 curve of Fig. 7 is used for the coil material in all cases considered.

In all results reported in the following paragraphs, the values of pressure P, moment M and curvature k are normalized by the yield pressure $P_Y = 2\sigma_Y t/D_m$, the fully-plastic moment $M_P = \sigma_Y D_m{}^2 t$, and the curvature-like parameter $k_I = t/D_m{}^2$, respectively, where σ_Y (490 MPa), D_m is the mean pipe nominal diameter ($D_m = D - t$) and t is pipe thickness.

4.1 Internally-pressurized bending capacity of spiral pipes

The effect of spiral forming process on pressurized bending capacity is examined for both the 36-inch and 48-inch diameter pipes, described in section 3.2 and tested experimentally. An imperfection is used, in the form of initial wrinkling, with an amplitude equal to 1% and 4% respectively, as measured in the corresponding specimens. After spiral forming, a hydrotest step

is performed, before the application of internal pressure, at a level of 72% of yield pressure. Subsequently keeping the pressure constant, bending is applied. This loading procedure is similar to the one followed in the experiments and is most likely to occur during a geohazard action. Curvature k of the bent specimen is defined equal to $8\delta/L^2$, where the length L and the mid-span displacement δ are shown schematically in Fig. 23. For the case of 36-inch-diameter pipe the model which used for the parametric study considers a different length L=10.39D with respect to the model presented in section 3, while for the case of 48-inch-diameter pipe the same model presented in section 3 is used.

Fig. 24 (a) shows the moment-curvature diagrams from three spiral pipes, with different coil diameter ("NU" case). In order to explain the effect of diameter coil in pressurized-bending response, the stress-strain response of the pipe after the forming process and hydrotest is also obtained and is shown in Fig. 24 (b) at a representative location on the outer surface of the pipe after hydrotest. The results indicate that decreasing coil diameter, the yield stress decreases, and this is attributed to the influence of Baushinger effect, which is more pronounced at large strains. The moment-curvature diagrams can be correlated with the corresponding stress-strain behavior; decreasing values of coil diameter imply a decrease of yield stress because of Bauschinger effect, and this results on smaller values of bending moment capacity.

Besides bending moment capacity, the critical curvature $k_{\max}$ is an essential parameter for pipeline design. In the present paper, it is defined as the curvature at which maximum moment $M_{\max}$ occurs. The results show that smaller values of coil diameter correspond to higher values of critical curvature. Fig. 8 shows that the decrease of coil diameter results in an increase of plastic deformation and hardening, and this explains the increase of critical curvature value.

The effect of "unloading" ("NU" versus "U") on the bending capacity is also examined. To explain structural behavior, the stress-strain response at a specific location is obtained, accounting for forming process and hydrotest. Fig. 25 (a) shows the moment-curvature response for the "U" and "NU" cases and Fig. 25 (b) shows the axial stress-strain behavior at a location on the outer surface of the pipe. The results demonstrate that, for the "U" case,

yield stress is lower but hardening is higher. Furthermore, Fig. 25 shows that the presence of "unloading" results in higher values of critical bending curvature (due to increased hardening) but lower values of maximum bending moment (due to yield stress reduction). Fig. 26 (a) shows the moment-curvature response of two 36-inch-diameter pipes without "unloading" ("NU" case); the first pipe has been subjected to hydrotest after the forming process, whereas the second pipe has not been subjected to hydrotest. The stress-strain behavior shown in Fig. 26 (b), indicates that hydrotest results in higher values of yield stress, so that the moment capacity is increased. On the other hand, the corresponding critical curvature is lower, due to lower hardening. For the 48-inch-diameter pipe, similar simulations are performed; two coil diameters are examined, and the results, presented in Fig. 27 to Fig. 29, show a similar response with the 36-inch-diameter pipe.

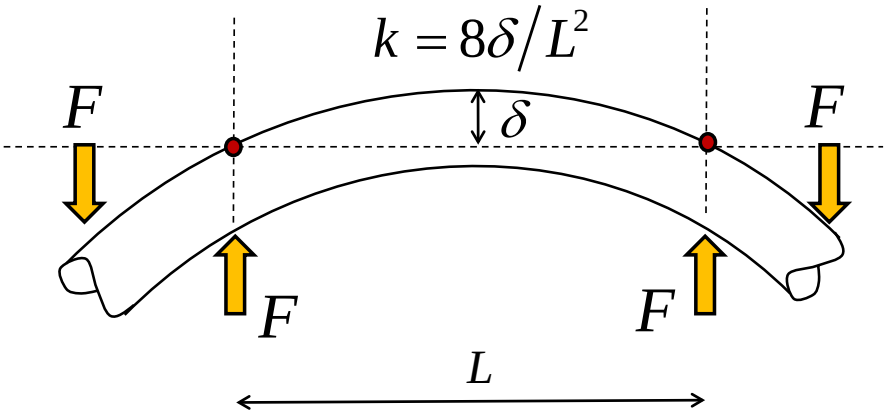

Fig. 23: Schematic representation of the four-point bending scheme, and calculation of bending curvature.

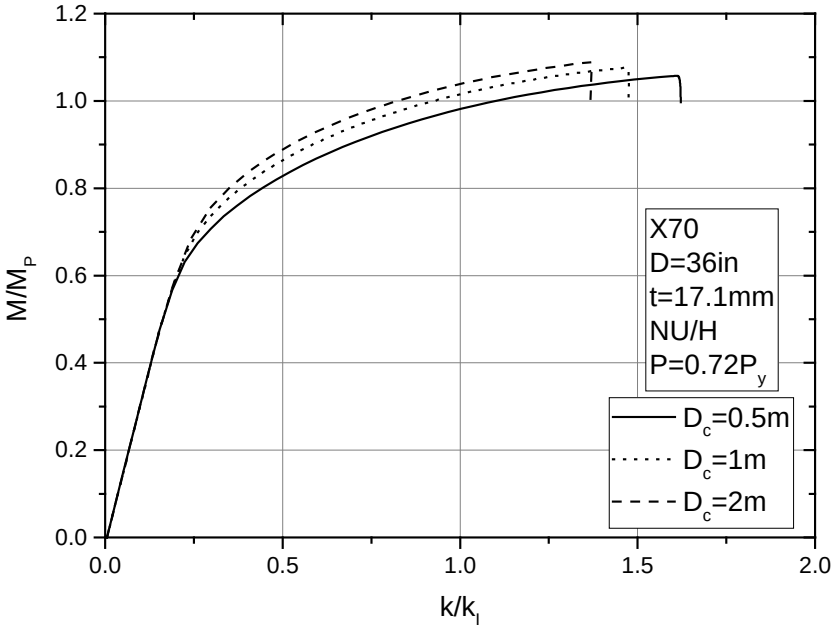

(a)

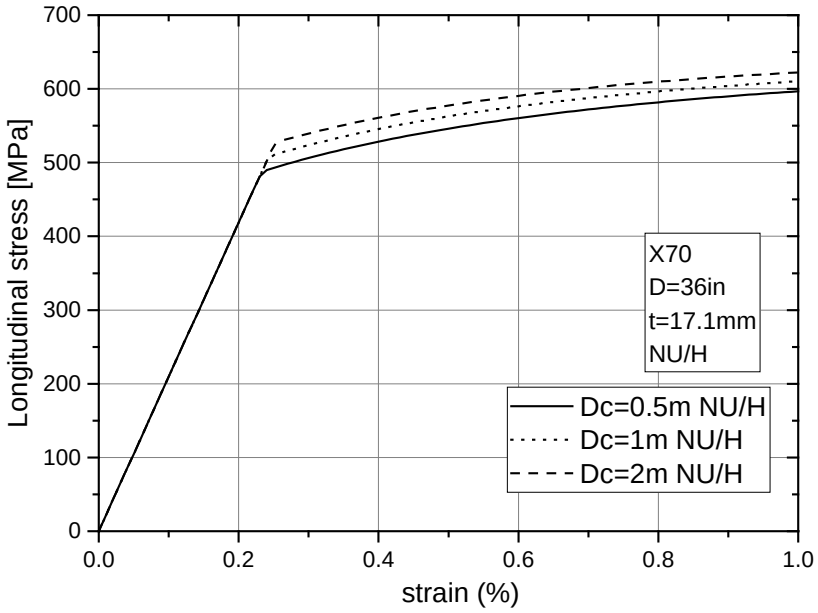

(b)

Fig. 24: (a) Moment-curvature diagrams for 36-inch-diameter pipe (NU/H case) for three different coil diameters under internal pressure $P/P_y = 0.72$; (b) stress-strain diagram (after hydrotest before structural load or pressure application) for three values of coil diameter.

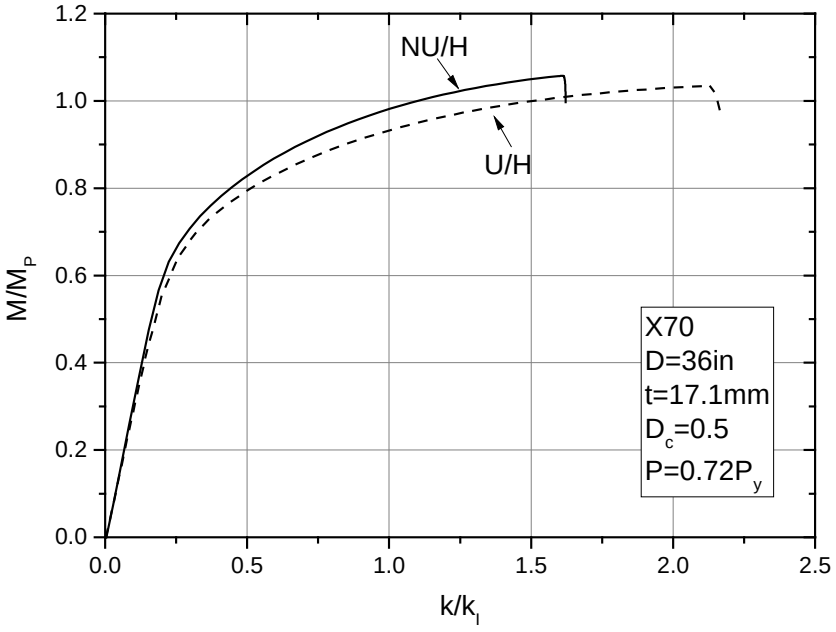

(a)

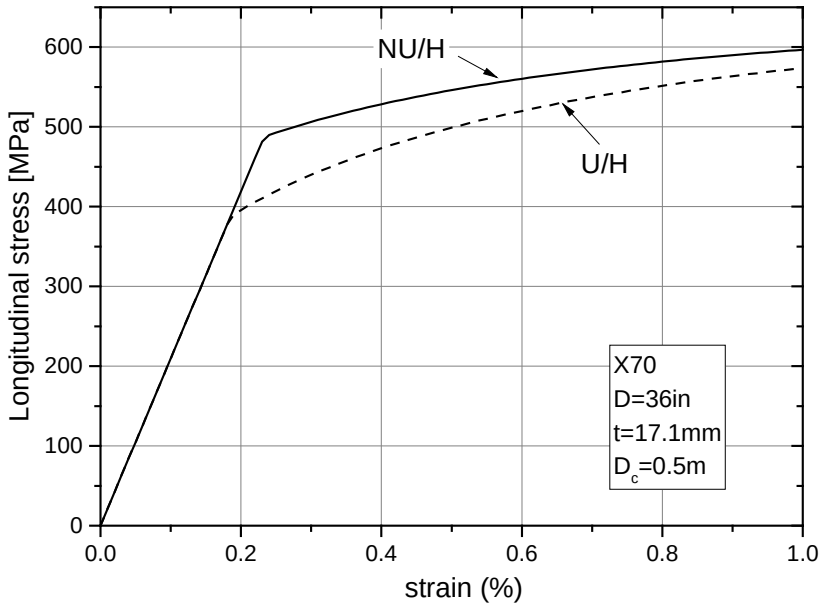

(b)

Fig. 25: (a) Moment-curvature diagrams for 36-inch-diameter pipe with and without "unloading"; internal pressure is equal to 72% of P_y; (b) stress-strain diagram (after hydrotest before structural load or pressure application) with and without "unloading" at the spiral forming process.

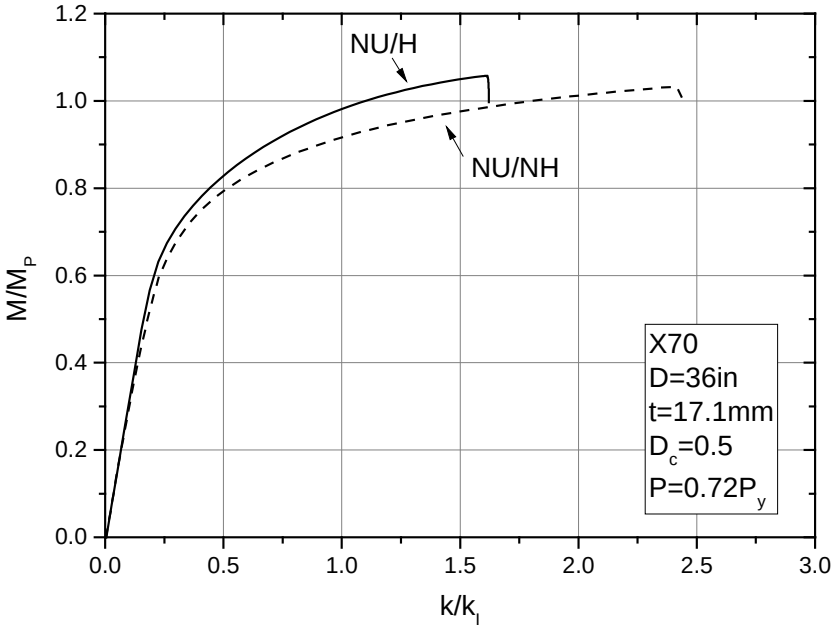

(a)

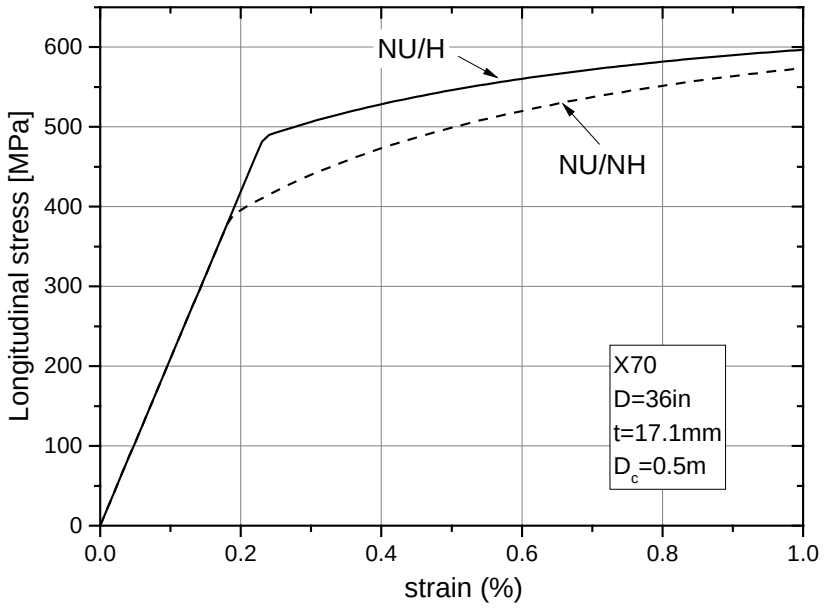

(b)

Fig. 26: (a) Moment-curvature diagrams for 36-inch-diameter pipe with and without hydrotest (without "unloading") under internal pressure equal to 72% of P_y; (b) stress-strain after spiral forming (no "unloading"), with and without hydrotest .

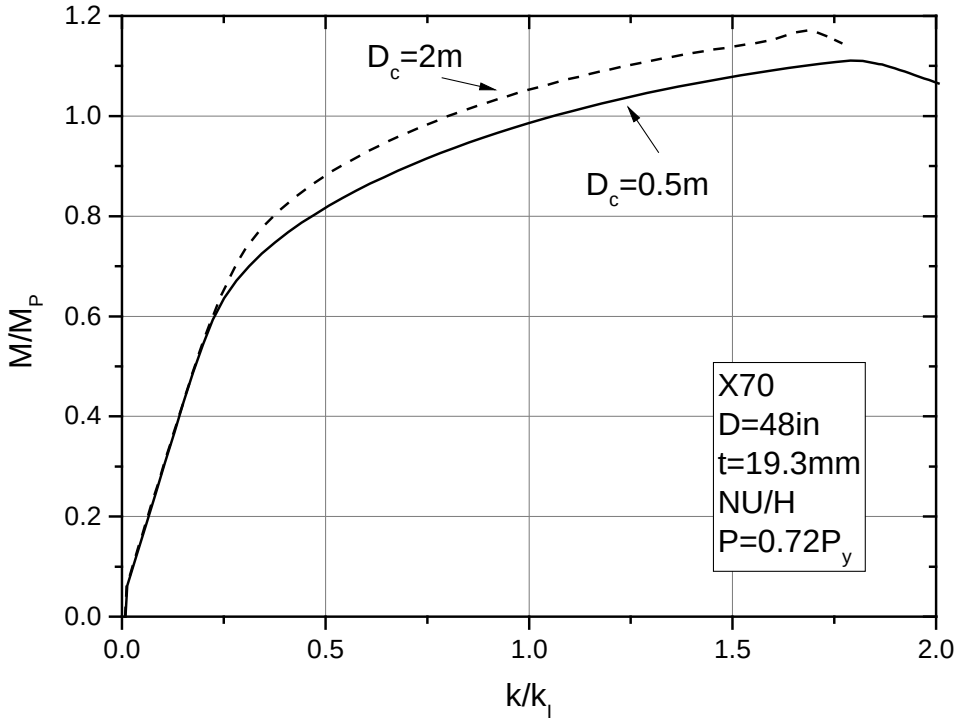

Fig. 27: Moment-curvature diagrams for a 48-inch-diameter X70 spiral pipe, considering two different coil diameters (internal pressure $P / P_y = 0.72$).

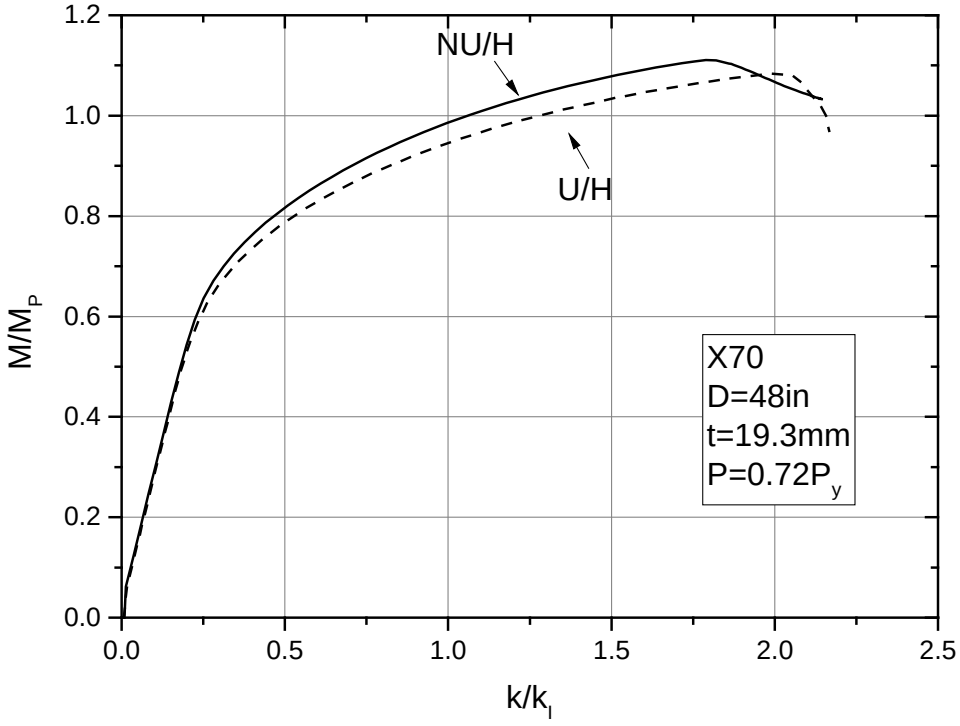

Fig. 28: Moment-curvature diagrams for a 48-inch-diameter spiral pipe after hydrotest, with and without "unloading", (internal pressure $P / P_y = 0.72$).

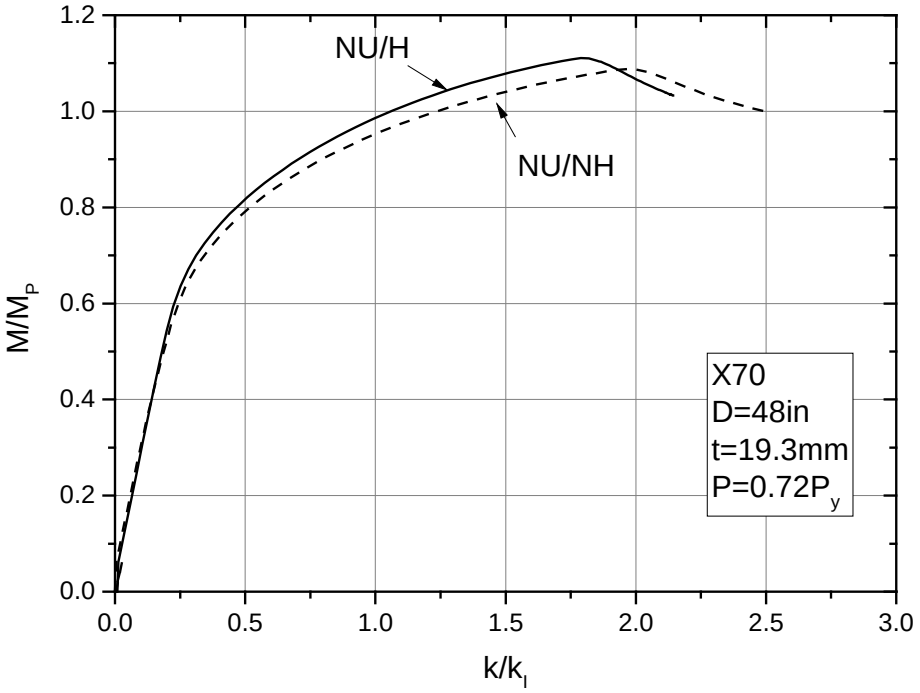

Fig. 29: Moment-curvature diagrams for a 48-inch-diameter pipe with and without hydrotest ("NU" case, internal pressure $P/P_y = 0.72$).

4.2 External pressure collapse resistance

A 28-inch-diameter pipe, similar to the specimen tested under external pressure, as described in section 3.1, is considered in the present paragraph. The pipe has thickness equal to 18mm and has been subjected to external pressure after hydrotest. An initial ovality of 2.5% is used, which is the maximum allowable value specified in the BS 8010 standard for offshore pipelines [20]. A 15 diameter-long pipe segment is considered, so that pressure response is independent of the presence of end caps. Fig. 30 summarizes the results of the parametric analysis in terms of coil diameter size and "unloading" after spiral bending. The results show that coil diameter does not affect significantly external pressure capacity. Fig. 31 depicts the compression stress-strain response in the hoop direction after hydrotest, for three values of coil diameter ("NU" case) at a representative location on the outer surface of the pipe away from the spiral weld. The three diagrams show a similar uniaxial compressive stress-strain response and this explains the insignificant effect of coil diameter D_c on the collapse pressure.

On the other hand, the results in Fig. 30 show that hydrotesting has a pronounced effect on the ultimate pressure capacity, hydrotesting increases substantially the collapse pressure. This behavior is attributed to the fact that during hydrotest, residual stresses are significantly decreased. This is shown in Fig. 32 and Fig. 33 for coil diameter D_c equal to 1m. Similar response is observed for all values of D_c. Fig. 34 depicts the compressive stress-strain response of the pipes with and without hydrotest ("NU" case), and indicates that the compression yield stress is higher when hydrotest is applied.

The effects of "unloading" after the spiral bending ("NU" versus "U") on pressure capacity is also depicted in Fig. 30. One should notice that in all cases hydrotest reduces residual stresses. For the case of "NH" the effect of "unloading" after the spiral forming is more dominant than the case in which hydrotest exists. The existence of unloading when the hydrotest is omitted seems to increase the collapse pressure due to the fact that the yield stress for "U/NH" case is lower than the "NU/NH" case as shown in Fig. 34.

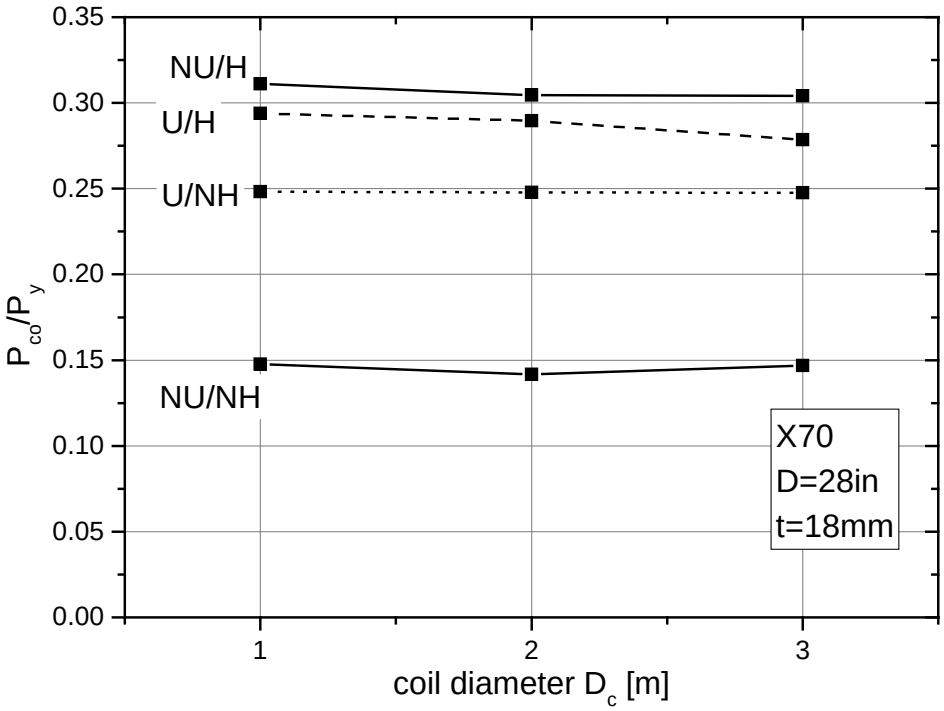

Fig. 30: Collapse pressure variation in terms of coil diameter D_c for different cases of "hydrotest" and "unloading".

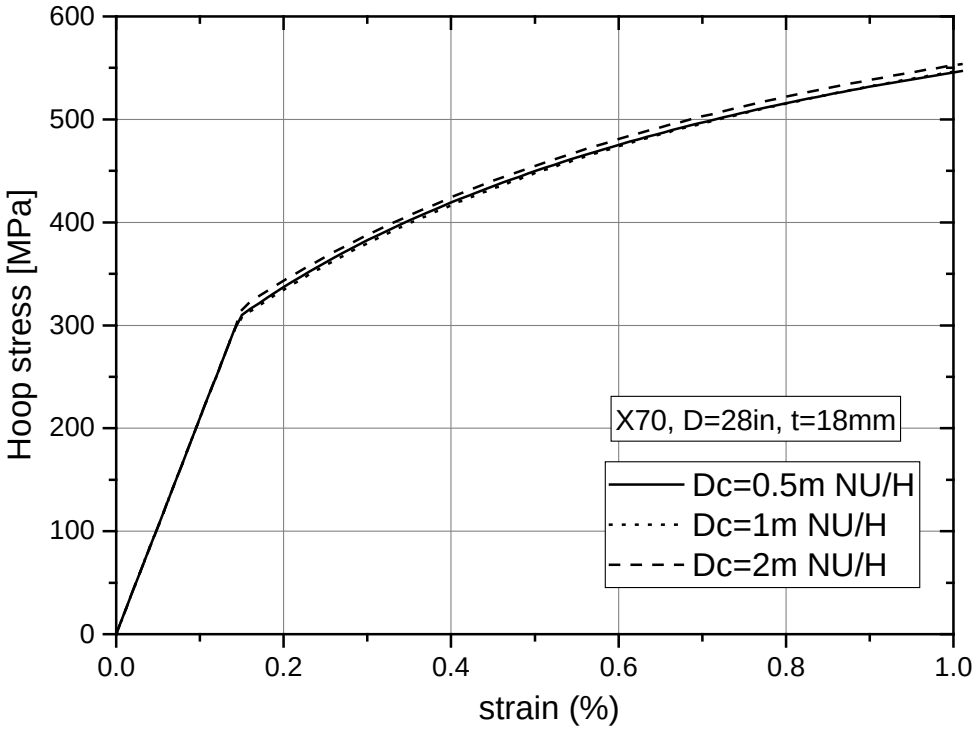

Fig. 31: Compressive stress-strain response in hoop direction for three diameters of coil ("NU/NH" case).

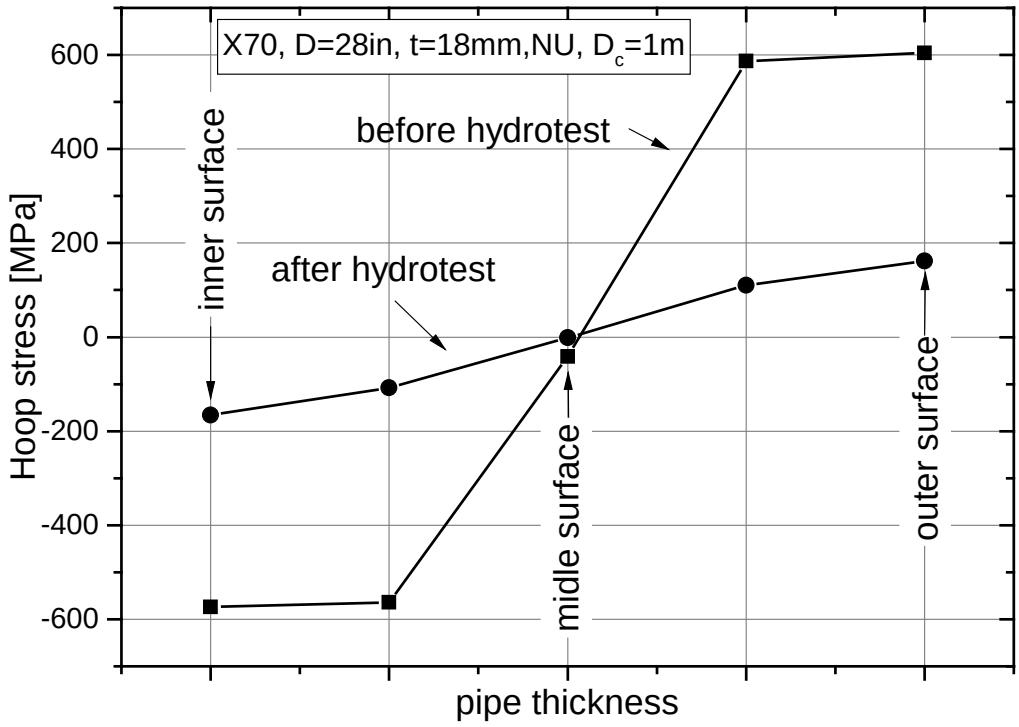

Fig. 32: Residual stresses distribution in the hoop direction across pipe thickness before and after hydrotesting (no "unloading", "NU" case).

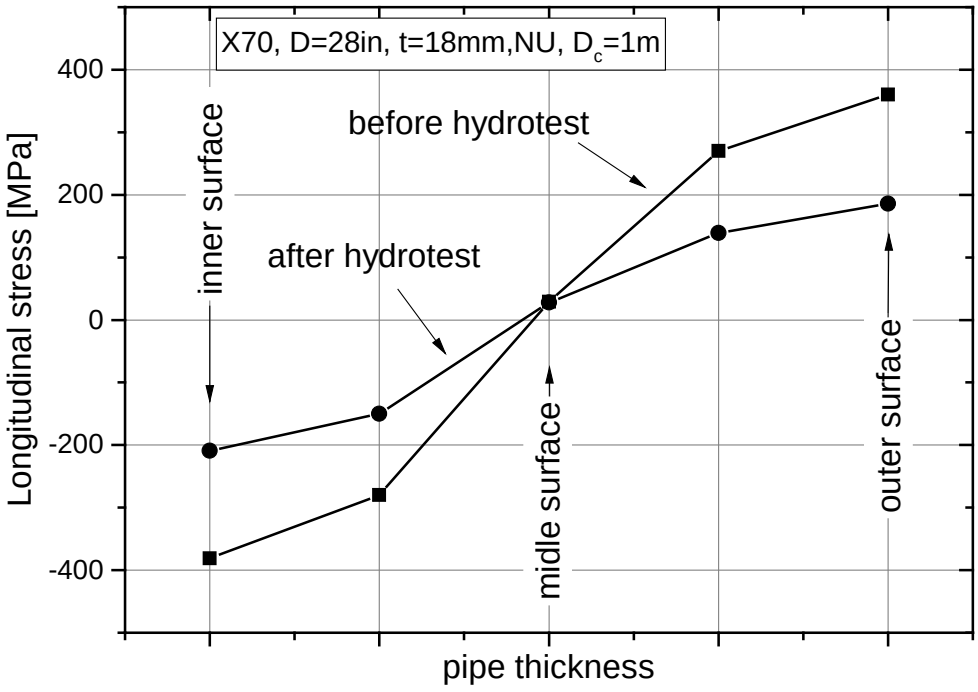

Fig. 33: Residual stresses distribution in the longitudinal direction across pipe thickness before and after hydrotesting (no "unloading" "NU" case).

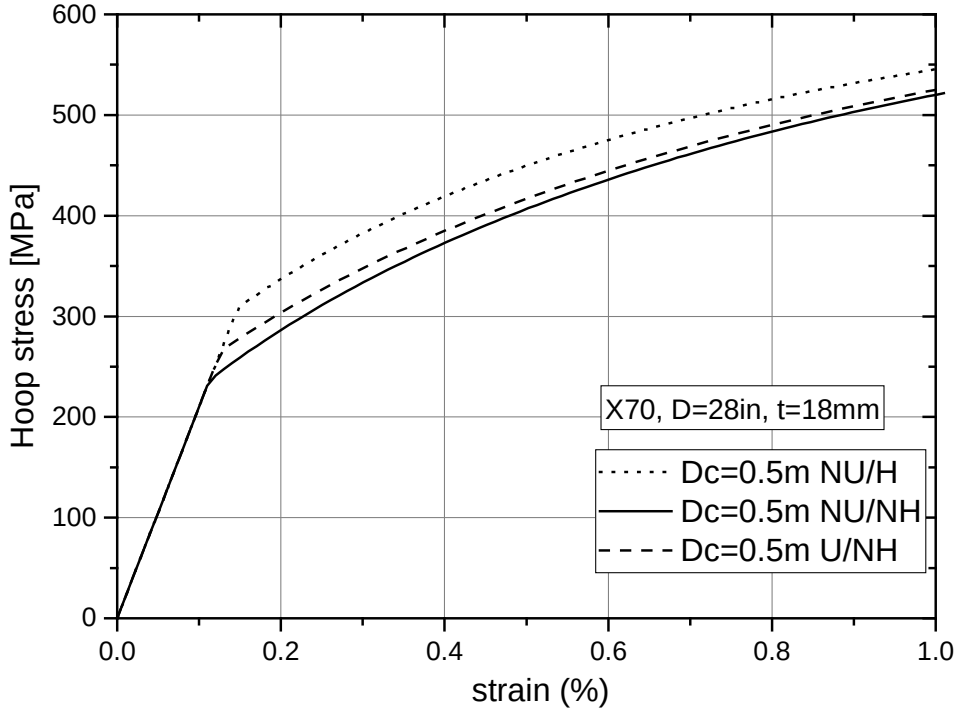

Fig. 34: Stress-strain response in the hoop direction of a point located at the inner diameter of coil (D_c=0.5m), for different cases regarding "unloading" and "hydrotest".

5 CONCLUSIONS

The spiral cold bending manufacturing process and its effect on the structural performance of spiral pipes have been studied using advanced finite element simulation tools. Numerical models simulating both decoiling and spiral bending have been presented, using two finite element approaches. Subsequently, using the spiral bending manufacturing results as initial conditions, the structural response of the pipes has been studied using a structural model of the spiral pipe. The numerical tools have been validated against experimental results on four pipe specimens: a 36-inch-diameter pipe and two 48-inch-diameter pipes (all three subjected to four-point bending in the presence of internal pressure), and a 28-inch-diameter pipe (subjected to external pressure). The good comparison between numerical and experimental results built confidence in the numerical tools.

After model validation, a parametric analysis has been conducted, focusing on the effect of manufacturing process on structural behavior, considering the influence of coil diameter, the pressure of "unloading" during the spiral bending process, and the effect of hydrotest. For the case of pipes, subjected to internally-pressurized bending, the study concluded that the decrease of the value of coil diameter has a rather small negative effect on the maximum bending moment, but the corresponding critical curvature is somewhat increased due to hardening associated with decoiling. The existence of "unloading" has a moderate influence on the structural response, while "hydrotest" has negligible effects.

For the 28-inch-diameter pipe, analyzed under pure external pressure, the present study concluded that the value of coil diameter has negligible influence and there exists a moderate effect in the case where "unloading" is allowed. Furthermore, the results have indicated that hydrotest has a significant positive effect on the collapse pressure, because of residual stress reduction.

The results from the present study have been used to support the argument that spiral-welded pipes are capable of sustaining significantly amount of bending deformation prior to local buckling. This indicates that spiral-welded pipes constitute promising candidates for demanding onshore applications (e.g. geohazard areas), and for moderately-deep offshore

pipeline applications. For a detailed discussion of this argument, considering also tensile failure modes, the reader is referred to the final report of the SBD-SPIPE project [12].

ACKNOWLEDGEMENTS

The research work described in this paper was carried out with a financial grant from the European Commission through the Research Fund for Coal and Steel, Contract RFSR-CT-2013-00025, *Strain-Based Design of Spiral-Welded Pipes for Demanding Pipeline Applications*, acronym SBD-SPIPE. The contribution of Dr. Francesco Iob, Rina Consulting – Centro Sviluppo Materiali S.p.A., in the large-scale experiments is greatly appreciated. The authors would also like to thank Onderzoekscentrum Voor Aanwending Van Staal N.V (OCAS) and Dr. Steve Cooreman, in person, for providing the test data on the X70 steel coil material.

REFERENCES

[1] Bian, Y., Penniston, C., Collins, L., Mackenzie, R. (2010). "Evaluation of UOE and Spiral-Welded Line Pipe for Strain Based Designs". *Proceedings of the Biennial International Pipeline Conference*, IPC2010-31315, Calgary, Alberta, Canada.

[2] Zimmerman, T., Timms,, C., Xie, J, Asante, J. (2004). "Buckling Resistance of Large Diameter Spiral Welded Linepipe", *Proceedings of the International Pipeline Conference,* IPC 04, Calgary, Alberta, Canada.

[3] Van Es, S. H. J., Gresnigt, A. M., Kolstein, M. H., Bijlaard, F. S. K. (2013). "Local Buckling of Spirally Welded Tubes - Analysis of Imperfections and Physical Testing". *Proceedings of the International Offshore and Polar Engineering Conference*, ISOPE 2013, pp. 248-259, Anchorage, Alaska, USA.

[4] Van Es, S. H. J., Gresnigt, A. M., Vasilikis, D., Karamanos, S. A., (2016). "Ultimate bending capacity of spiral-welded steel tubes – Part I: Experiments". *Thin-Walled Structures,* Vol. 102, pp. 305-319.

[5] Van Es, S. H. J., Gresnigt, A. M., Kolstein, M. H., Bijlaard, F. S. K. (2014). "Strain Based Design of Spirally Welded Pipes, Local Buckling in 4-Point Bending". *Proceedings of the*

International Offshore and Polar Engineering Conference, ISOPE 2014, pp. 520-528, Busan, Korea.

[6] Eltaher, A., Jafri, S., Jukes, P., Heiberg, G. (2012). "Advanced Finite Element Analysis for Qualification of Spiral Welded Pipe for Offshore Application". *Proceedings of the International Offshore and Polar Engineering Conference*, ISOPE 2012, pp. 303-310, Rhodes, Greece.

[7] Zimmermann, S., Karbasian, H., Knoop, F. M. (2013). "Helical Submerged Arc Welded Line Pipe Engineered For Strain Based Design", *Proceedings of the International Offshore and Polar Engineering Conference*, ISOPE 2013, pp. 505-511, Anchorage, Alaska, USA.

[8] Nasim, K., Arif, A.F.M.,. Al-Nassar, Y.N, Anis, M. (2015). "Investigation of residual stress development in spiral welded pipe", *Journal of Materials Processing Technology,* Vol. 215, pp. 225–238.

[9] Forouzan, M.R., Mirfalah Nasiri, S.M., Mokhtari, A. Heidari, A., Golestaneh S. J. (2012), "Residual stress prediction in submerged arc welded spiral pipes" *Journal of Materials and Design,* Vol. 33, p.p. 384–394.

[10] Vasilikis, D., Karamanos, S. A., Van Es, S. H. J. and Gresnigt, A. M. (2016), "Ultimate Bending Capacity of Spiral-Welded Steel Tubes - Part II: Predictions", *Thin-Walled Structures*, Vol. 102, pp. 305-319.

[11] Van Minnebruggen, K., Hertelé, S., Thibaux, P., De Waele, W. (2015). "Effects of Specimen Geometry and Anisotropic Material Response on the Tensile Strain Capacity of Flawed Spiral Welded Pipes". *Engineering Fracture Mechanics*, Vol. 148, pp. 350–362.

[12] Mecozzi, E., *et al.* (2017), "Strain-Based Design of Spiral-Welded Pipes for Demanding Pipeline Applications", SBD-SPIPE project, RFSR-CT-2013-00025, *Final Report to European Commission*, Brussels.

[13] Chatzopoulou, G., Sarvanis, G. C., Papadaki, C. I., Karamanos, S. A. (2016). "The effect of Spiral Cold-Bending Manufacturing Process on Pipeline Mechanical Behavior", *Proceedings of the International Pipeline Conference*, IPC 2016, Calgary, Canada.

[14] Papadaki, C. I., Chatzopoulou, G., Sarvanis, G. C., Karamanos, S. A. (2018). "Buckling of internally-pressurized spiral-welded steel pipes under bending", *International Journal of Pressure Vessels and Piping*, Vol. 165, pp. 270-285.

[15] Armstrong, P.J., and Frederick, C.O., 1966. "A mathematical representation of the multiaxial Bauschinger effect", *CEGB Report* No. RD/B/N 731.

[16] Ucak, A., and Tsopelas, P., 2011. "Constitutive Model for Cyclic Response of Structural Steels with Yield Plateau", *Journal of Structural Engineering*, ASCE, Vol. 137, No. 2, pp. 195-206.

[17] Chatzopoulou, G., Karamanos, S. A., Varelis, G. E. (2016). "Finite Element Analysis of UOE Manufacturing Process and its Effect on Mechanical Behavior of Offshore Pipes", *International Journal of Solids and Structures,* Vol. 83, pp. 13-27.

[18] Kyriakides, S., Corona, E. (2007), *Mechanics of Offshore Pipelines*, Buckling and Collapse, Vol. 1, Elsevier.

[19] DNV OS-F101 (2012), *Submarine Pipeline Systems*, Oslo, Norway.

[20] BS 8010 (1993), *Code of practice for pipelines*. Part 3. Pipelines subsea: design, construction and installation.

[21] Limam, A., Lee, L.-H., Corona, E., Kyriakides, S., (2010), "Inelastic wrinkling and collapse of tubes under combined bending and internal pressure", *International Journal of Mechanical Sciences*, Vol. 52, No. 5, pp. 637-647.

[22] Suzuki, N., Tajika, H., Igi, S., Okatsu., M., Kondo, J., Arakawa, T., (2010), "Local Buckling Behavior of 48", X80 High-Strain Line Pipes", *Proceedings of the International Pipeline Conference*, IPC 2010, Calgary, Canada.